Myogenin is an Essential Regulator of Adult Myofibre Growth and Muscle Stem Cell Homeostasis

Massimo Ganassi[1*], Sara Badodi[2] , Kees Wanders[1] , Peter S. Zammit[1] , Simon M. Hughes[1*§].

[1]Randall Centre for Cell and Molecular Biophysics, King's College London, London, SE1 1UL, UK

[2] Blizard Institute, Barts and The London School of Medicine and Dentistry, Queen Mary University of London, 4 Newark Street, London E1 2AT, UK.

[*] Authors for correspondence s.hughes@kcl.ac.uk, m.ganassi@kcl.ac.uk

§ Lead author for correspondence

Keywords

Myog, zebrafish, myonuclei, skeletal muscle, Pax7, MuSC, Myostatin, IGF1, stem cell, Tsc1, TORC1

Abstract

Growth and maintenance of skeletal muscle fibres depend on coordinated activation and return to quiescence of resident muscle stem-cells (MuSCs). The transcription factor Myogenin (Myog) regulates myocyte fusion during development, but its role in adult myogenesis remains unclear. In contrast to mice, *myog*$^{-/-}$ zebrafish are viable, but have hypotrophic muscles. By isolating adult myofibres with associated MuSCs we found that *myog*$^{-/-}$ myofibres have severely reduced nuclear number, but increased myonuclear domain size. Expression of fusogenic genes is decreased, *pax7* upregulated, MuSCs are fivefold more numerous and mis-positioned throughout the length of *myog*$^{-/-}$ myofibers instead of localising at myofibre ends as in wild-type. Loss of Myog dysregulates mTORC1 signalling, resulting in an 'alerted' state of MuSCs, which display precocious activation and faster cell cycle entry ex vivo, concomitant with *myod* upregulation. Thus, beyond controlling myocyte fusion, Myog influences the MuSC:niche relationship, demonstrating a multi-level contribution to muscle homeostasis throughout life.

Introduction

Maintenance of adult skeletal muscle depends on the ability of multinucleated myofibres to grow and regenerate, thereby ensuring optimal functionality throughout life. To facilitate this homeostasis, adult vertebrate muscle own a specialised population of precursors cells, the muscle stem cells (MuSCs), also termed satellite cells, located between the basal lamina and sarcolemma of most adult myofibres (Mauro, 1961). Like other stem cells, MuSCs are mitotically dormant in normal circumstances but poised to respond to functional demand for new myonuclei throughout adult life (Purohit and Dhawan, 2019; Relaix and Zammit, 2012). The transcription factor Pax7 is considered a canonical quiescent MuSC marker across several vertebrate species and its expression is maintained during the progression to activation and proliferation, before downregulation at the onset of myogenic differentiation (Berberoglu et al., 2017; Buckingham and Relaix, 2015; Chen et al., 2006; Hammond et al., 2007; Hollway et al., 2007; Kawakami et al., 1997; Olguin and Olwin, 2004; Seale et al., 2000; Seger et al., 2011; Zammit et al., 2006). Null mutations for Pax7 severely affects MuSC maintenance and muscle regeneration in amniotes, amphibia and teleosts (Berberoglu et al., 2017; Chen et al., 2006; Oustanina et al., 2004; Relaix et al., 2006; Seale et al., 2000). In adult zebrafish,

Pax7^{+} MuSCs contribute to regeneration of myofibres upon muscle damage, being the functional counterparts of MuSCs in mammals (Berberoglu et al., 2017; Hollway et al., 2007; Pipalia et al., 2016).

Proper function of the MuSC pool depends on a dynamic balance between quiescence and activation and is sustained by feedback signalling from surrounding muscle (Forcina et al., 2019; Mashinchian et al., 2018). In response to stimuli, quiescent MuSCs activate and become muscle progenitor cells (MPCs), which proliferate, differentiate and fuse to contribute myonuclei to pre-existing multinucleated myofibres: a process that resembles aspects of myogenesis by embryonic myoblasts and relies on an intricate molecular network comprising both extrinsic and intrinsic mechanisms (Buckingham and Relaix, 2015). Among many converging factors, the members of the Myogenic Regulatory Factor (MRF) family of transcription factors, Myod, Myf5, Mrf4 and Myogenin (Myog), are key regulators of vertebrate muscle gene expression during both early and adult myogenesis (Hernandez-Hernandez et al., 2017; Zammit, 2017). In adult muscle, Myod and Myf5 are mainly expressed in MuSC and are crucial for efficient activation and proliferation (Cooper et al., 1999; Coutelle et al., 2001; Kuang et al., 2007; Megeney et al., 1996; Soleimani et al., 2012), whereas Mrf4 accumulates in mature myofibres and contribute to ensure their homeostatic growth (Moretti et al., 2016; Voytik et al., 1993).

Knockout of the *Myog* gene in mouse leads to severe muscle deficiencies and, in contrast to the other members, is neonatal lethal (Hasty et al., 1993; Nabeshima et al., 1993), thus making difficult to investigate Myog function in detail. As in embryogenesis, Myog expression is upregulated in proliferating MuSCs that then rapidly undergo myogenic differentiation (Zammit et al., 2004) and its expression appears reciprocally balanced with that of Pax7 (Olguin and Olwin, 2004; Olguin et al., 2007; Riuzzi et al., 2014; Zammit et al., 2006). However, depletion of mouse *Myog* in myoblasts does not block accumulation of differentiation markers in vitro, but cell biological aspects such as myotube formation were not explored (Meadows et al., 2008). We recently expanded this observation reporting that, despite being dispensable for myogenic differentiation, Myog is essential for myocyte fusion and its functional depletion leads to formation of mononucleated myofibres and reduced myotome growth during zebrafish embryo/larvae stage (Ganassi et al., 2018). Moreover, modulation of rodent Myog expression shifts muscle enzyme activity towards oxidative metabolism, alters exercise capacity and is required for neurogenic atrophy (Ekmark et al., 2003; Flynn et al., 2010; Hughes et al., 1999; Meadows et al., 2008; Moresi et al., 2010), suggesting a broad Myog role in regulating adult muscle homeostasis. Nevertheless, whether Myog acts on myofibre, MuSC or both has remained elusive.

Importantly, in contrast to mouse, zebrafish *myog*$^{-/-}$ mutant adult fish are alive albeit displaying hypotrophic muscle (Ganassi et al., 2018). Congruent with the fish phenotype, almost complete depletion of mouse *Myog* after birth results in decreased muscle size (Knapp et al., 2006; Meadows et al., 2008), thereby confirming a conserved vertebrate role for Myog in regulating bulk muscle growth and maintenance.

Here, to explore the role of Myog in adult muscle, we analysed *myog*$^{-/-}$ mutant zebrafish and deployed our recently-developed method to isolate viable single myofibres with associated MuSCs, allowing culture of muscle progenitor cells (MPCs). Morphometric analysis revealed that *myog*$^{-/-}$ muscle has reduced myofibre growth and nuclear accretion compared to siblings (sibs), revealing increased myonuclear domain size. Adult *myog*$^{-/-}$ muscle exhibited upregulation of *pax7a* and *pax7b* expression along with supernumerary MuSCs, that were randomly distributed throughout myofibre length compared to sib MuSCs, which localise mainly at

myofibre ends, suggesting an altered MuSC niche. Ex vivo analysis of *myog*$^{-/-}$ MuSCs revealed elevated phosphorylation of ribosomal protein S6, concomitant with reduced expression of the mTOR inhibitor *tsc1*, indicating enhanced mTORC1 activity, which marks MuSCs that left deep quiescence to enter into an 'alert' pseudo-activated state (Rodgers et al., 2014). Congruently, cultured myofibres from mutants yielded increased numbers of MPCs with an accelerated proliferative phase, marked by upregulated expression of *pax7a*, *pax7b* and *myod*. Together, our study demonstrates that Myog plays a crucial role in adult muscle growth and MuSC homeostasis.

Results

Adult *myog*$^{-/-}$ myofibres are small with fewer nuclei but increased nuclear domain size

Adult zebrafish bearing the *myog*^{kg125} nonsense mutant allele (*myog*$^{-/-}$), which reduces *myog* mRNA, eliminates Myog protein and is presumed null, are viable but have reduced muscle bulk (Ganassi et al., 2018). In contrast, *myog*$^{kg125/+}$ heterozygous siblings (sib) are indistinguishable from wild-type sibs and are used as paired controls throughout the current study. Gene expression analysis on dissected adult trunk muscle confirmed continued significant downregulation of *myog* mRNA in *myog*$^{-/-}$ fish compared to co-reared sib controls (Figure 1A,B) in line with the nonsense-mediated decay reported previously (Ganassi et al., 2018). Levels of mRNA encoded by the terminal myogenesis genes *mymk*, *mymx* and *mrf4* were downregulated by 52%, 38% and 68% respectively in *myog*$^{-/-}$ compare to the relative expression in sib, as during the embryonic stage, suggesting a continuous muscle defect in adulthood (Figure 1B). To explore further the muscle defect at a cellular level, we isolated single myofibres from juvenile (1 mpf; months post fertilisation) and adult (8 mpf) *myog*$^{-/-}$ and sibs (Figure 1C). Both juvenile adult mutant myofibres were on average 20% and 50% shorter than those in control, respectively, demonstrating an early onset growth deficit in *myog*$^{-/-}$, with lifecourse worsening (Figures 1C,D and S1A,B). Despite significant 50% reduction in overall fibre length, sarcomere length was unaffected in adult *myog*$^{-/-}$ myofibres, as in embryonic myofibres (Figure 1E) (Ganassi et al., 2018). In contrast, myofibres isolated from the adult hypomorphic *myog*^{fh265} mutants (Hinits et al., 2011, Ganassi et al., 2018) were indistinguishable from those of age-matched sibs (Figure S1C). The number of nuclei associated with each isolated myofibre appeared greatly reduced in *myog*$^{-/-}$ mutants compared to sibs (Figures 1F and S1D). Indeed, nuclear numbers per unit length were reduced fourfold in mutants (Figure 1G). Congruently, calculation of the average number of nuclei associated with each adult myofibre by multiplying the number of nuclei/unit length by the length yielded revealed an approximate 90% reduction, from an average of 95 nuclei per myofibre in sibs to nearly 12 nuclei per myofibre in *myog*$^{-/-}$ (Figure 1H). Numbers of total nuclei in *myog*$^{-/-}$ myofibres was reduced similarly at juvenile stage compared to sibs (Figure S1D). Juvenile sib myofibres had significantly more nuclei than adult *myog*$^{-/-}$ myofibres, confirming ongoing myonuclear accretion defect in *myog*$^{-/-}$ (Figures 1H and S1D). Thus, *myog*$^{-/-}$ mutant myofibres are grossly defective and show no sign of homeostatic recovery over time.

Further morphometric analysis revealed that lack of Myog led to an average persistent decrease of 40% in myofibre diameter resulting in 50% reduction of myofibre surface area, compared to age-matched juvenile and adult sib, respectively (Figures 1F,I and S1E). Indeed, as expected, the surface area per myofibre nucleus (surface area domain size; SADS) was increased by almost threefold in *myog*$^{-/-}$ (Figure 1J) indicating both inadequate nuclear accretion, congruent with suppression of *mymk* and *mymx* mRNAs (Figure 1B), and a compensatory increase in SADS, which remained larger in mutants throughout life, showing no sign of return

to a normal size as mutants age. Nevertheless, both genotypes displayed significant increase in both myofibre diameter, surface area (SA) and number of nuclei between juvenile and adult stages, indicating ongoing muscle growth (Figures 1G,I and S1E). However, although myofibre SA and number of nuclei positively correlated in *myog*$^{-/-}$, we observed a reduced nuclear accretion as myofibres get larger area compared to sib, hence highlighting a significantly different growth mode among the two genotypes (different trend slopes) (Figure 1K). Coherently, the incremental increase in myofibre SA over the juvenile-to-adult time-frame was significantly reduced in *myog*$^{-/-}$, confirming a persistent deficit in muscle growth (Figure 1L). Thus, loss of Myog function affects normal muscle growth, impinging on size and nuclear accretion of myofibres.

Adult *myog*$^{-/-}$ myofibres have increased number of MuSCs

Isolated myofibres have two kinds of associated nuclei, genuine muscle fibre nuclei and nuclei of resident MuSCs. To assess MuSC abundance in *myog*$^{-/-}$, we first analysed *pax3* and *pax7* mRNAs, well-known markers of MuSCs (Buckingham and Relaix, 2015; Hammond et al., 2007; Pipalia et al., 2016). Gene expression analysis on whole muscle showed upregulation of *pax7a* and *pax7b* mRNAs of 82% and 120%, respectively, in *myog*$^{-/-}$ compared to control sibs, but no change in *pax3a* or *pax3b* (Figures 2A and S2A). *Myf5* mRNA, a marker of partially-activated or 'alerted' MuSCs in mice and MPCs in fish, and known to be a Pax7 target gene (Coutelle et al., 2001; Kuang et al., 2007; Soleimani et al., 2012), was upregulated by over 200%, further suggesting an increase of MuSCs number in *myog*$^{-/-}$. In contrast, *myod* mRNA, a marker of fully-activated proliferating MuSCs (Megeney et al., 1996; Zammit et al., 2004; Zammit et al., 2002), was unaltered (Figure 2A). These data raise the possibility that *myog*$^{-/-}$ adults have alterations in MuSCs. To facilitate identification of *bona fide* MuSCs, *myog*$^{kg125/+}$ fish were bred onto *pax7a*:*GFP* reporter and MuSCs identified by GFP fluorescence (Figure 2B,C;(Mahalwar et al., 2014; Pipalia et al., 2016)). Immunostaining of GFP^{+ve} cells with the DP312 antibody, that recognises fish Pax3/Pax7 (Davis et al., 2005; Hammond et al., 2007), confirmed MuSC identity (Figure 2D). Adult *pax7a*:*GFP;myog*$^{-/-}$ fish showed reduced muscle compared to co-reared *pax7a*:*GFP;myog*$^{+/-}$ sibs (Figure S2B), replicating the phenotype on a wild-type background (Ganassi et al., 2018). Upon muscle dissociation, we observed that single *myog*$^{-/-}$ myofibres bore around five GFP^{+ve} cells on average, compared to only one on sib myofibres (Figure 2E). Indeed, almost 40% of nuclei associated with *myog*$^{-/-}$ myofibres were in GFP^{+ve} cells compared to less than 2% in sib (Figures 2G and S2C). Thus, MuSCs are more abundant in *myog*$^{-/-}$ mutants than in sibs. Subtraction of MuSC nuclei from the total nuclei associated with isolated adult myofibres, revealed that sib myofibres have over thirteenfold more genuine myofibre nuclei (i.e. myonuclei) than *myog*$^{-/-}$ myofibres (Figure S2D). These GFP^{-ve} myonuclei allowed calculation of a myofibre volume per true myonucleus, the notional myonuclear domain. In line with SADS, the myonuclear domain was increased by 2.3-fold in *myog*$^{-/-}$ fibres (Figure 2F), despite the 7.8-fold reduction in absolute myofibre volume (Figure S2E). Accordingly, corrected SADS showed an increase of almost fivefold (Figure S2F). Thus, Myog in the adult suppresses muscle growth, by limiting both nuclear domain size and MuSC number.

Altered MuSC:niche relation in *myog*$^{-/-}$ mutant myofibres

Myofibres from *myog*$^{-/-}$ showed a striking set of alterations in MuSC distribution. In control sib, MuSCs were found mostly localised close to the myofibre end, whereas in *myog*$^{-/-}$ the supernumerary MuSCs were randomly distributed along the myofibre length (Figure 2H and S2G). In sibs, 70% of myofibres had a single associated MuSC, which was usually within 20 µm from the myofibre end (Figures 2G,I,J and S2G,H). In contrast, only

33% of myofibres had a single MuSC in mutants (Figures 2G,I and S2G,H), which displayed consistent random location, often far from the myofibre end (Figure 2I,J). Around 60% of *myog*$^{-/-}$ myofibres bore two or more MuSCs, whereas only 9% of sib myofibres had two or more MuSCs, and none had over three (Figure 2G). Strikingly, 21% percent of sib myofibres had no GFP^{+ve} cells, compared to only 5% of *myog*$^{-/-}$ myofibres (Figure 2G and S2G). The results suggest that lack of Myog either enhances MuSC proliferation, prevents MuSC differentiation or both. Data in this and the preceding section demonstrate that lack of Myog alters MuSC number, position and expression of stemness marker genes, suggestive of an alteration in their relationship to their normal myofibre end niche.

Lack of Myog enhances mTORC1 signalling in adult muscle and MuSCs

To investigate further how Myog may influence the MuSC niche, we assessed the expression of factors that contribute to muscle growth via regulation of MuSC activation. Whole muscle analysis revealed 130% increased level of *igf1* mRNA and nearly 50% downregulation of *myostatin b* (*mstnb*) mRNA, both regulators of muscle growth and the mTORC1 (mechanistic Target Of Rapamycin Complex 1) pathway (Trendelenburg et al., 2009; Yoon, 2017), suggesting that lack of Myog triggers a growth signalling response (Figure 3A,B). In contrast, expression of the zebrafish IGF1 receptors, *igfr1a* and *igfr1b* was unaltered (Figure S3A) indicating that *myog*$^{-/-}$ myofibres, and/or MuSCs, may respond to the higher IGF1 level similarly to sib. IGF1 signalling involves phosphorylation of AKT that activates mTORC1 resulting in downstream events such as promotion of muscle growth, accompanied by phosphorylation of the ribosomal protein S6 (RPS6) (Figure 3C and (Ruvinsky et al., 2009; Yoon, 2017). Western blot analysis of whole muscle extracts revealed that whereas AKT phosphorylation at Ser473 (pAKT) appeared unchanged, downstream phosphorylation of RPS6 at Ser240/244 (pRPS6) was enhanced fourfold in *myog*$^{-/-}$ muscle compared to sib (Figure 3D). Phosphorylation of RPS6 (pRPS6) marks the onset of MuSC activation in vivo (Rodgers et al., 2014). Thus, we analysed pRPS6 level in MuSCs on freshly-isolated myofibres from *pax7a:GFP*;*myog*$^{-/-}$ or control *pax7a:GFP*;*myog*$^{+/-}$ sib. *Myog*$^{-/-}$ MuSCs showed a robust twofold increase in pRPS6 level (Figure 3E,F), in line with quantification in whole muscle. No change was detected in myofibres themselves. As pRPS6 was increased but pAKT was not similarly altered, we reasoned that lack of Myog might control the expression level of factors that inhibit the mTORC1 pathway. Tsc1 and Tsc2 form a stabilised GTPase complex that represses the mTOR cascade (Figure 3C; (Nobukini and Thomas, 2004). Levels of *tsc1a* and *tsc1a* mRNAs were reduced by 51% and 57%, respectively, in *myog*$^{-/-}$ muscle, whereas *tsc2* mRNA was unchanged compare to sib (Figure 3G), consistent with increased pRPS6. We conclude that lack of Myog triggers activation of the mTORC1 pathway in MuSCs, concomitant with *Tsc1a/b* repression, leading to precocious MuSC activation.

Adult *myog*$^{-/-}$ MuSC-derived myoblasts exhibit faster transition to proliferation

To assess MuSC activation and proliferation potential, myofibres bearing GFP^{+ve} cells, from either *pax7a:GFP*;*myog*$^{-/-}$ or control *pax7a:GFP*;*myog*$^{+/-}$ sib were individually plated, cultured for 4 days in growth medium and the number of associated myogenic cells counted (Figure S3B). *Myog*$^{-/-}$ mutants yielded at least three times as many mononucleate cells than did sibs (Figure S3B), paralleling the increased number of MuSCs on freshly-isolated myofibres. The vast majority (80-90%) of cells from fish of either genotype was GFP^{+ve}, so *bona fide* MPCs. *Myog*$^{-/-}$ myofibres also displayed an average threefold increased GFP^{+ve} cell yield compared to sibs (Figure 4A-C). Within the 4 day culture period, sib myofibres (70% of which had only a single

GFP^{+ve} MuSC) yielded around 40 MuSCs, reflecting a mean doubling time of around 20 h. Mutants yielded a slightly higher proportion of GFP^{+ve} MPCs than sibs (Figure 4C), perhaps reflecting the increased number of MuSCs on each myofibre and the upregulation of *pax7a* mRNA in *myog*$^{-/-}$ muscle. Importantly, although both genotypes yielded a GFP^{-ve} cell population, all cells immunoreacted for Desmin, confirming their myogenic identity (Figure S3B). Notably, the relative MPC proliferation rates were not significantly different among genotypes, calculated as the ratio of the number of GFP^{+ve} MPCs obtained after 4 days in culture to the average number of GFP^{+ve} MuSC per myofibres (Figure 4D). We conclude, that *myog*$^{-/-}$ mutant and sib MuSCs have similar proliferative potentiality when assayed in culture.

To explore proliferation dynamics further, MPCs were pulsed with EdU at either 2, 3 or 4 days ex vivo after myofibre plating in growth medium (Figure 4E). To increase MPC yield for downstream analyses, 90-100 fibres were plated per well (Figures 4E and S3C). As expected, *myog*$^{-/-}$ myofibres yielded more MPCs after 2 days in culture compared to sibs, and both genotypes produced mainly Desmin^{+ve} muscle lineage cells (Figure S3C,D). EdU pulse 2 days after plating revealed striking differences between *myog*$^{-/-}$ MPCs, 60% of which were EdU^{+ve}, compared to sib MPCs, only 20% of which incorporated EdU (Figure 4E,F). A day later (on day 3), the difference in proliferation had reversed; sib MPCs were almost 60% EdU^{+ve}, whereas incorporation into *myog*$^{-/-}$ MPCs was significantly reduced compared to both sibs on day 3 and *myog*$^{-/-}$ MPCs on day 2 (Fig. 4E,F). This difference in S-phase labelling between *myog*$^{-/-}$ and sib MPCs persisted on day 4 (Figure 4E,F). Statistical analysis of overall EdU incorporation dynamics as Area Under Curve (AUC) revealed slightly higher proliferation rate of sib MPCs (Figure 4E). We conclude that MPCs in *myog*$^{-/-}$ mutants are more readily driven into proliferation upon release from their in vivo environment.

We next explored MuSC dynamics by analysing MPCs mRNA levels at day 2 and day 3 of culture. Both *pax7a* and *pax7b* were more abundant, fourfold and threefold, respectively, in *myog*$^{-/-}$ MPCs at 2 days compared to sib (Figure 4G), consistent with the higher percentage of MuSCs observed (Figure 4C). Strikingly, while *pax7a* mRNA reduced with time, *pax7b* mRNA was maintained at similar level between day 2 and day 3 across genotypes, despite confirming overall increased level in *myog*$^{-/-}$ MPCs (Figure 4G). Moreover, *myod* mRNA was fifteenfold more abundant in *myog*$^{-/-}$ MPCs compared to sib, again suggesting an earlier entry into activation phase. Notably, higher *myod* expression in *myog*$^{-/-}$ MPCs lasted into day 3. In contrast, *myf5* mRNA level appeared similar in *myog*$^{-/-}$ and sib MPCs at both 2 and 3 days, although tending to decrease at the later timepoint (Figure 4G). The data suggest that *myog*$^{-/-}$ MPCs show faster activation and greater recovery from a stem-like state than MPCs from sibs.

The decreased proliferation but enhanced *myod* mRNA in cultured *myog*$^{-/-}$ compared to sib MPCs also suggested that the mutant cultures might be entering the terminal differentiation program. We assessed onset of differentiation by analysing expression of *mef2d* and *mylpfa* (encoding a fast myosin light chain), crucial players in myogenesis, which revealed significantly higher levels of both mRNAs in *myog*$^{-/-}$ relative to sib MPCs with an approximate upregulation of *mefd2d* and *mylpfa* by twofold and sixtyfold, respectively (Figure 4H). Immunostaining confirmed accumulation of sarcomeric myosin heavy chain (MyHC) and significantly higher differentiation index in *myog*$^{-/-}$ compared to sib MPCs, despite the continued exposure to growth medium (Figure 4I). Altogether, our data indicate that while Myog function is dispensable for MPC proliferation and terminal differentiation, its lack either prevents MuSCs achieving full quiescence or accelerates MuSC transition into the proliferation phase, suggesting that Myog contributes to maintaining the MuSC niche.

Discussion

Here we describe a novel function for the transcription factor Myog in regulating adult skeletal muscle growth rate and MuSC dynamics through four major findings. First, Myog influences MuSC number. Second, Myog is required for MuSCs to adopt their normal niche position. Third, Myog contributes to MuSC deep quiescence, regulating expression of genes involved in mTORC1 signalling. Lastly, Myog is required for proper myofibre growth and myonuclear accretion throughout life.

Myog controls MuSC number

We show that *myog*$^{-/-}$ mutation causes supernumerary MuSCs/MPCs, paralleled by increased *pax7a* and *pax7b* mRNA. In addition to the fivefold increase in MuSC/adult myofibre and 50% reduction in myofibre length reported here, we previously described that adult *myog*$^{-/-}$ mutants have unaltered body length and numbers of myofibre profiles/transverse body section roughly equal to their non-mutant siblings (Ganassi et al., 2018). Taken together, these data suggest that total number of Pax7^{+} MuSCs is increased around tenfold in adult *myog*$^{-/-}$ mutant myotome. In mouse, expression of Pax7 and Myog in MuSC appear to be mutually exclusive and controlled through reciprocal inhibition in in-vitro studies (Olguin et al., 2007; Riuzzi et al., 2014). Persistent *Pax7* expression delays Myog accumulation in cultured myoblasts and ex vivo in MuSCs on myofibres, while silencing of *Myog* can result in retention of *Pax7* expression in differentiation (Olguin et al., 2007; Zammit et al., 2006). As Myog is required for adult myoblast fusion in vitro (Ganassi et al., 2018) and *mymk* and *mymx* mRNAs are reduced in adult *myog*$^{-/-}$ muscle, one must consider the possibility that some *pax7a:GFP*$^{+ve}$ mononucleate cells are not MuSCs but differentiated myocytes that retain the *pax7a* reporter and are unable to fuse. However, we detect Pax3/7 protein in MuSCs, showing that strong GFP accumulation is not just perdurance of earlier signal. Moreover, most *myog*$^{-/-}$ MuSCs enter into S-phase after 2 days ex vivo. Subsequently, *myog*$^{-/-}$ MPCs quickly up-regulate the differentiation marker *mylpfa* sixtyfold, suggesting that an insignificant fraction was previously terminally differentiated. In addition, *myog*$^{-/-}$ muscle expresses more *myf5*, a MPC marker. In post-natal rodent muscle, *Myf5* is expressed in MuSCs, not myofibres (Beauchamp et al., 2000). Like our finding, murine *Myog*-knockout also led to *Myf5* accumulation in neonatal limb muscle, even though one-third of the total nuclei are still MuSCs/MPCs in wild type neonates (Cardasis and Cooper, 1975; Rawls et al., 1998). Taken together, these data argue that the abundant *pax7a:GFP*$^{+ve}$ cells are MuSCs or MPCs.

We consider two possible hypotheses for the increased number of MuSC/MPCs in *myog*$^{-/-}$ mutants; differentiation failure or active accumulation. We do not favour the idea that absence of Myog prevents MPCs undergoing terminal differentiation leading to the accumulation of cells blocked in differentiation for three reasons. First, *myog*$^{-/-}$ MPCs readily undergo differentiation in culture and during myogenesis in the embryo (Ganassi et al., 2018). Second, although muscle is reduced in size, there is enough formed to support life and sarcomere length is unaffected, so terminal differentiation is fairly efficient without Myog during larval and adult growth and any required muscle repair. Third, both in fish and amniotes, MPCs ready to differentiate express high levels of Myod, which acts in a feedforward mechanism to trigger cell cycle exit and Myog expression (Hinits et al., 2009; Weintraub et al., 1991). We do not, however, observe increased levels of *myod* mRNA in *myog*$^{-/-}$ mutant muscle. Nevertheless, when *myog*$^{-/-}$ MPCs are placed in culture they dramatically upregulate *myod*, arguing that Myod upregulation is also a characteristic of adult zebrafish MPC differentiation. Active

accumulation of MuSCs, on the other hand, is suggested by the increase in *pax7a*, *pax7b* and *myf5* mRNAs in *myog*$^{-/-}$ mutant muscle. Below, we raise the hypothesis that the abundance of myofibres with low numbers of nuclei may trigger MuSC accumulation as a homeostatic response to tissue insufficiency.

Myog is required for MuSCs to adopt their normal niche position

In wild-type fish 21% of myofibres have no associated MuSCs, despite having around 95 myofibre nuclei. This finding strongly argues that, in order to grow or repair damage, MuSC/MPCs must migrate across the basal lamina between fibres, as occurs in developing rodent muscle (Hughes and Blau, 1990). We observe 0.92 MuSCs/wild-type myofibre, on average. If one assumes random MuSC distribution amongst myofibres, the Poisson distribution predicts that 40% of myofibres should have no associated-MuSCs. The lower proportion of myofibres lacking MuSCs suggests that MuSCs are not distributed randomly. Conversely, Poissonian distribution would predict that 37% of myofibres should have a single MuSC. The observed value of 70% strongly suggests that MuSCs actively disperse between myofibres. Nevertheless, the system is imperfect, as the 21% of myofibres lacking MuSCs shows. Despite the fivefold increase in MuSCs in *myog*$^{-/-}$ mutant, around 5% of myofibres still have no associated MuSC, which is far more than expected by the Poisson distribution (1.5%). Similarly, the 33% of myofibres with only a single MuSC compares with an expected value of 6%. In contrast, myofibres with over ten MuSCs are over-represented, perhaps due to rare local regenerative events. In the absence of Myog, MuSCs tend to cluster on some myofibres, while also showing a tendency to be present at just one per myofibre more often than expected. These observations raise the possibility that myofibres in both wild-type and *myog*$^{-/-}$ mutant contain a single specific niche for MuSCs.

Most MuSCs associated with isolated myofibres in zebrafish are located near myofibre ends, which would be attached to the vertical myoseptum tendon-like structure in vivo. It thus appears that the myotendinous junction (MTJ) at myofibre ends provides a special niche in which MuSCs accumulate. Strikingly, the preferred location of MuSCs in wild-type myofibres is between 10-20 μm from the myofibre end, suggesting that MuSCs locate not on the MTJ surface itself, but on the immediately adjacent cylindrical sarcolemma, retaining a potential physical contact with the MTJ. Upon explant ex vivo, MuSCs activate and begin to migrate away from myofibre ends. In *myog*$^{-/-}$ mutants, the increased number of MuSCs are almost randomly distributed along the fibre, but the slightly higher abundance at myofibre ends might suggest that cells disperse once the MTJ niche is filled. However, when the fraction of myofibres in *myog*$^{-/-}$ mutants that have only a single MuSC were analysed separately, significant dispersal was still observed. We conclude that Myog is required for assembly of the MTJ MuSC:niche complex.

Mammalian MuSCs are generally not associated with myofibre ends, perhaps because myofibres are longer. Zebrafish myofibres are on average 1 mm long and rarely exceed 2 mm. In contrast, in the murine muscles most frequently analysed, those of the limbs, myofibres are up to 1 cm long. We suggest that the more numerous nuclei and larger number of MuSCs required for efficient growth and repair have allowed (or selected for) the MuSC niche to disperse along the myofibre.

Myog contributes to MuSC deep quiescence

Numerous lines of evidence argue that MuSCs in *myog*$^{-/-}$ zebrafish fail to enter full quiescence. First, MuSCs are more numerous in *myog*$^{-/-}$ mutant adults. Second, they are often not in their normal niche. Third, they contain more pRPS6 upon acute isolation. Fourth, they activate and proliferate more rapidly upon ex vivo

culture. Three hypotheses could explain the MuSC *myog*$^{-/-}$ phenotype. 1) Lack of Myog function in early development. However, MuSCs are not increased in mutant larvae (Ganassi et al., 2018) so it seems the defect worsens over the life course, suggesting a continuous need for Myog. 2) Lack of Myog within myofibre nuclei, which might lead to signals promoting MuSC proliferation (see below). 3) Myog could also function within MuSC themselves to control the balance between quiescence and activation. Whereas most literature describes *Myog* expression at the differentiation step following MuSC proliferation, various reports that noted Myog^{+} MuSCs support a Myog MuSC-specific function. An early study investigating differential expression of *Myod* and *Myog* in rat muscle observed rare but intense accumulation of Myog mRNA along myofibre edges, anatomically reminiscent of MuSC niche (Hughes et al., 1993). Notably, Myog expression predominates in oxidative myofibres also characterized by higher MuSC density (Gibson and Schultz, 1982; Hughes et al., 1993). Rantanen et al. identified a population of dormant Myog^{+} MuSCs which may contribute to muscle repair bypassing the proliferation step (Rantanen et al., 1995). Co-expression of Pax7 and Myog was observed in a satellite-cell study in transverse sections of both mouse soleus and EDL muscles (Schultz et al., 2006) and in rare cells in fish dermomyotome (Devoto et al., 2006). Likewise, immunohistochemistry on human resting muscle biopsies found *Myog* expression in MuSC but not in myonuclei (Lindstrom et al., 2010). More recently, the Blau group reported a low but detectable level of Myog protein in both resting murine MuSCs and in MPCs returning to quiescence after recovery from injury (Porpiglia et al., 2017). In addition, datasets show that *Myog* mRNA is present in quiescent MuSCs and rapidly decreases significantly during the three hours of myofibre isolation (Machado et al., 2017). Interestingly, *Mrf4* expression in MuSC was downregulated in the same time frame, concomitant with exit from quiescence marked by the upregulation of *Myod*, demonstrating the presence of two well-known muscle 'differentiation-specific' markers in dormant stem cells. Together, such observations prompt re-evaluation of an intrinsic Myog function in quiescent MuSC.

Myog is required for proper myofibre growth

MRFs including Myog are required in the adult to restrict murine myofibre size (Moresi et al., 2010; Moretti et al., 2016). We find that, in zebrafish, Myog is required both for myocyte fusion that permits increase in nuclear number and consequent growth to the normal fibre size. We also show that Myog limits myonuclear domain size both in juvenile and adult muscle. Conditional depletion of Myog in adult mouse muscle decreased myofibre cross-sectional area, although further morphometric analysis of myofibre nuclear domains was not reported (Meadows et al., 2008). It therefore seems that, in addition to its role in promoting MPC differentiation and fusion, Myog restricts the volume of sarcoplasm supported by each myonucleus, both in denervated (Moresi et al., 2010) and innervated (this study) adult muscle. Both adult mouse and zebrafish *Myog* mutants show reduction in *Mrf4* mRNA (Ganassi et al., 2018; Knapp et al., 2006; Meadows et al., 2008; Rawls et al., 1998; Venuti et al., 1995). Mrf4 itself restricts murine myofibre growth (Moretti et al., 2016), although no myofibre size change was reported in the various *Mrf4* knockout mice (Patapoutian et al., 1995; Zhang et al., 1995). So Myog may either restrict myonuclear domain size directly or by regulating *Mrf4* expression.

Unlike fish, which grow to some extent throughout life, mice do not require MuSCs to maintain adult muscle size (Keefe et al., 2015). Nevertheless, during murine adult myogenesis myonuclear accretion from MuSC-derived MPC fusion is required for myofibre growth and regeneration, as in fish (Pallafacchina et al., 2013). Congruently, expression of fusogenic genes *myomixer* (*mymx*) and *myomaker* (*mymk*) is reduced in both *myog*$^{-/-}$ adult and embryonic muscles (Ganassi et al., 2018). Depletion of zebrafish Mymk leads to fewer

myofibre nuclei in the surviving adults (Shi et al., 2018). Likewise, *Mymk*-KO in murine MuSCs at P0 led to 75% reduction of myonuclear number in extensor digitorum longus (EDL) myofibres measured at P28 (Nikolaou et al., 2019). Although severely reduced, accretion of myonuclei does occur in growing *myog*$^{-/-}$ zebrafish, thus confirming the persistence of a Myog-independent pathway to fusion (Ganassi et al., 2018), which appears to allow a fraction of MPCs to sustain some muscle growth.

Addition of myonuclei to growing muscle relies on interactive signals between MuSCs and myofibres. Fish lacking Myog have increased *igf1* and decreased *mstnb* expression. Both changes are predicted to enhance muscle size (Coleman et al., 1995; Durieux et al., 2007; Gao et al., 2016; McPherron et al., 1997; Powell-Braxton et al., 1993; Trendelenburg et al., 2009; Zimmers et al., 2002), and both may be important in our *myog* mutants. As we observe in *myog*$^{-/-}$ fish, loss of Mstn increases MuSCs in amniotes (Manceau et al., 2008; McCroskery et al., 2003). MuSC contribution is, however, dispensable for myofibre hypertrophy in *Mstn* knockout mice, in which growth derives from increased myonuclear domain size. *Mstn* knockouts thus resemble both the MuSC increase and myofibre domain size increase in *myog* mutant fish. On the other hand, IGF1 has been shown to increase MPC proliferation and differentiation and thereby enhance myofibre growth, but without change in nuclear domain size (Fiorotto et al., 2003; McCall et al., 1998). *Igf1* increase might thus enhance the number of MuSCs in *myog* mutants.

IGF1 and Myostatin signalling also affect MuSC activation status in mice (Chakravarthy et al., 2001; Cornelison and Wold, 1997; McCroskery et al., 2003; Zhang et al., 2010). Both can act through the mTORC1 pathway (Latres et al., 2005; Trendelenburg et al., 2009). The IGF1 signal cascade phosphorylates AKT and activates mTORC1 leading to phosphorylation of RPS6 and eIF4EBPs, with downstream effects on both MuSCs and adult myofibres (Schiaffino and Mammucari, 2011). Loss of Mstn also activates the mTORC1/RPS6 pathway (Trendelenburg et al., 2009). Our data show enhanced RPS6 phosphorylation (pRPS6) both in *myog*$^{-/-}$ muscle and MuSC analysis ex vivo. Interestingly, mTORC1 controls the transition from deep G_0 quiescence to an intermediate pseudo-activated state defined as G_{alert}, in which MuSCs that accumulate pRPS6 are primed for activation compared to their quiescent counterparts (Porpiglia et al., 2017; Rodgers et al., 2014). Similar to zebrafish *myog*$^{-/-}$ MuSCs, “alerted” mouse MuSCs display accelerated transition to proliferation ex-vivo compared to quiescent population (Rodgers et al., 2014). As we detected no difference in Akt activation and unaltered levels of the receptors *igfr1a* and *igfr1b*, we deduce that increased phosphorylation of RPS6 is unlikely to result from enhanced upstream IGF1 cascade. However, *myog*$^{-/-}$ muscle showed significant downregulation of *tsc1a* and *tsc1b* mRNAs, that encode functional orthologues of mammalian TSC1, a mTORC1 inhibitor highly conserved from fly to human (DiBella et al., 2009; Nobukini and Thomas, 2004) that promotes stemness in various tissues (Chen et al., 2008; Quan et al., 2013). Mouse Tsc$^{-/-}$ MuSCs display enhanced pRPS6 and accelerated entry into proliferative state in vivo and in vitro (Rodgers et al., 2014). Murine Myog can bind to conserved regions in *Tsc1* gene, whereas Myod does not, thus suggesting direct transcriptional regulation (https://www.encodeproject.org/experiments/ENCSR000AID/). These observations raise the hypothesis that loss of Myog leads to mTORC1 activation in MuSCs, exit from G_0 into G_{alert} and subsequent increase in MuSC number. Taken together, our findings suggest that loss of Myog acts in adult animals to influence both MuSCs and muscle fibres, thus acting as a coordinator of tissue homeostasis.

Materials and methods

411

412 **Zebrafish lines and maintenance**

413 All lines used were reared at King's College London on a 14/10 hours light/ dark cycle at 28.5 °C, with staging
414 and husbandry as described (Westerfield, 2000). *myog*^{fh265} mutant allele were maintained on AB background
415 and genotyped by sequencing as previously described (Hinits et al., 2011; Roy et al., 2017). *Myog*^{kg125} (*myog*$^{-/-}$)
416 were made by CRISPR/Cas9, genotyped as previously reported and maintained on TL background (Ganassi
417 et al., 2018). *TgBAC(pax7a:GFP)*^{t32239Tg}, a generous gift from Nüsslein-Volhard C. (MPI Tübingen) (Mahalwar
418 et al., 2014), and the newly-generated *myog*^{kg125}*;TgBAC(pax7a:GFP)*^{t32239Tg} were maintained on AB
419 background. All experiments were performed on zebrafish derived from F2 or later filial generation, in
420 accordance with licences held under the UK Animals (Scientific Procedures) Act 1986 and later modifications
421 and conforming to all relevant guidelines and regulations. Adult zebrafish measurement and analysis of weight,
422 length, body mass index and standard weight were performed as previously described (Ganassi et al., 2018).

423

424 **Isolation of zebrafish myofibres and culture of MuSCs from adult tissue**

425 Isolation and culture of zebrafish adult muscle fibres was previously described (Ganassi et al., 2018). Zebrafish
426 aged 8-9 months (adult) or 1 month (juvenile) were culled in high dose tricaine (Sigma Aldrich), immersed for
427 5 min in 1% Virkon (3S Healthcare) diluted in dH_2O, washed in PBS for 5 min followed by 70% ethanol rinse,
428 eviscerated and skinned. 15 month old adult were used for the *myog*^{fh265} allele. For myofibre dissociation, trunk
429 muscle was incubated in 0.2% Collagenase (C0130, Sigma Aldrich), 1% Penicillin/Streptomycin DMEM
430 supplemented with 50 µg/ml gentamycin (Thermo Fisher) at 28.5 °C for at least two hours. Single muscle
431 myofibres were released by trituration using heat-polished glass pipettes and washed three times with DMEM
432 Glutamax High Glucose (Gibco). Myofibres were then imaged for total length measure or plated on Matrigel
433 (Invitrogen) coated 96 or 24 well plates and cultured in growth medium (20% Fetal Bovine Serum in 1%
434 Penicillin/Streptomycin/ DMEM GlutaMAX High Glucose supplemented with 10 µg/ml gentamycin). At
435 indicated time points, MPCs were washed twice with PBS to remove plated myofibres, EdU pulsed (10 µM,
436 Invitrogen Life Technologies) for 8 hours in fresh media and then fixed with 4% PFA for 15 minutes. For
437 immunostaining myofibres were fixed in 4% PFA in PBS immediately after dissociation to reduce processing
438 time and avoid MuSC activation.

439

440 **Myofibre morphometry and Growth mode analysis**

441 Absolute myofibre length was measured for viable (i.e. non-fixed) myofibres imaged immediately after isolation
442 on Leica M stereo-microscope using x1.6 magnification. Measurement of Surface Area (SA) and number of
443 nuclei was performed on fixed myofibres at x10 or x20 magnification using an Axiovert 200M microscope
444 (Zeiss). Myofibre diameter was measured at two locations over total myofibre length. Morphometric calculation
445 were carried out as described in (Brack et al., 2005). Briefly, SA/unit length = myofibre segment length x π x
446 mean myofibre diameter; surface area domain size (SADS) = SA/myofibre nuclei in segment (Hoechst^{+ve});
447 Myofibre volume/unit length= myofibre segment length x π x (radius)^2; myonuclear domain= myofibre segment
448 length x π x (radius)^2 /myonuclei (i.e. GFP^{-ve} nuclei) in segment. MuSC (GFP^{+ve} cell) distance to nearest
449 myofibre-end was measured as schematised in Figure S2G. To graph frequency distribution, absolute nearest
450 myofibre-end distances were normalised for myofibre length difference across genotype. Each myofibre was
451 virtually divided in tenths where 1/10 and 5/10 corresponded to nearest segment to myofibre-end or segment

at the myofibre half-length, respectively. Each tenth measured either 100 µm in sib or 50 µm in *myog*$^{-/-}$.

Generalised linear models (GLS) were used to explore growth assessing genotype differences in the relationship between SA and number of nuclei per 100 µm length (NoN), using the GLS function of NMLE package in R version 3.6.1 "Action of the Toes" (https://www.R-project.org/, (Pinheiro, 2020)). SA was $\log_e$-transformed prior to analysis to generate a linear relationship with NoN, in a dataset pooling both juvenile and adult data. The dependent variable was set as NoN and the model included main effects of $\log_e$(SA) and genotype, as well as an interaction term. The dataset was then split by genotype and separate GLS models were run to analyse the relationship between $\log_e$(SA) and NoN for each genotype. *t*, *p* and DF values were extracted for these models with the 'summary' function and were as follow:

- Interaction between genotype and $\log_e$(SA): t=7.332, p<0.0001, DF=1,164
- Siblings only, effect of $\log_e$(SA): t=11.448, p<0.0001, DF=1,97
- Mutants only, effect of $\log_e$(SA): t=4.515, p<0.0001, DF=1,67

Detailed steps of the GLS analysis are reported:

- Decision to pool age groups

Initial analyses showed no effect of age on the relationship between $\log_e$(SA) and NoN, therefore different age groups were pooled to study the effect of mutation. Note that these initial analyses suffered from high confounding correlation between SA and age in siblings, however visual analysis of the few datapoints where juvenile and adult SA values overlapped gave no indication that age was affecting the NoN directly.

- Decision to use Generalised Linear Model instead of General Linear Model

Significant heteroscedasticity was identified in simple linear models using R package lmtest (Zeileis, 2002), primarily because variance in NoN increased with $\log_e$(SA). GLS models were used to weight explained variance by the value of the dependent variables, controlling for this heteroscedasticity. For each step of analysis every combination of weighting (weighting by $\log_e$(SA), genotype, both, or neither) was compared and the model with the lowest AIC was selected.

- Issue of Correlation between $\log_e$(SA) and Genotype

In the final model there was a significant correlation between explanatory variables $\log_e$(SA) and genotype, which may have confounded interpretations. This correlation was removed by subsetting with the 'Matchit' and 'Matching' R packages, and qualitatively identical results were found by re-running the analysis using this smaller dataset (Ho, 2011; Sekhon, 2011).

Protein extraction and Western blot analysis

Western blot was performed as described (Ganassi et al., 2014; Kelu et al., 2019). Briefly, dissected trunk muscle was submerged in lysis buffer (Tissue Extraction Reagent I (Invitrogen), Complete EDTA-free Protease Inhibitor Cocktail Tablets (Roche), 1mM PMSF, 50 mM NaF, 1mM Na_3VO_4 (Sigma Aldrich) and triturated using TissueRuptor (Qiagen) followed by 5 min of sonication. Lysates were then pelleted by centrifugation, after which the supernatant protein extract was quantified, mixed with Laemmli Sample Buffer 4X (Bio-rad) complemented with 2-mercaptoethanol (Bio-rad) and heated at 95 ºC for 5 minutes, before subjecting to SDS-PAGE analysis. Protein extract equivalent to 50 µg was loaded per lane onto precast gradient gels (4-20% Bio-rad). Separated proteins were then transferred to nitrocellulose membranes, blocked in either 5% non-fat dry milk or 5% BSA in Tris-buffered saline and 0.1% Tween (TBST), incubated in primary and secondary antibodies at 4ºC overnight and at room temperature for 2 hours, respectively. Primary antibodies used were:

S6 ribosomal protein (pan) (1:1000; #2317; Cell Signaling), phospho-S6 ribosomal protein (Ser240/244) (1:2000; #5364; Cell Signaling), Phospho-Akt (Ser473) 1:1000; #4051; Cell Signaling, Akt (pan) (1:1000; #4685; Cell Signaling), Actin (1:500; #A5316; Sigma Aldrich). Secondary antibodies used were: HRP goat anti mouse IgG(H+L) (1:5000; #AP308P; Sigma Aldrich) and HRP goat anti rabbit IgG (H+L) (1:5000; #AP307P; Sigma Aldrich). Signal detection was performed using ChemiDoc Imaging System and analysed on Image Lab Software (Bio-rad). Phospho/pan (total) ratios were calculated following normalisation to membrane-matched and sample-matched Actin signals.

Immunostaining on myofibres or cultured MPCs

For immunostaining, either myofibres or MPCs were permeabilised in PBS 0.5% Triton X-100 (PBST) for 15 min, blocked in Goat Serum 5% (Sigma Aldrich) in PBST and incubated with primary antibodies at indicated concentrations overnight in Goat Serum 2% in either PBST (0.1% TritonX) (myofibres) or PBS (MPCs). Primary antibodies used were against: phospho-S6 ribosomal protein (Ser240/244), (1:1000; #5364; Cell Signaling), GFP (13970 (1:400), Abcam), Myosin (A4.1025 (1:5) (Blagden et al., 1997), MF20 (1:300, DSHB), Pax3/7 (DP312 (1:50), Nipam Patel, UC Berkeley, USA) and Desmin (D8281 (1:100), Sigma Aldrich). Samples were then washed three times in PBS prior to incubation with secondary antibodies in Goat Serum 2% in PBS. Secondary antibodies were Alexa Fluor 555 goat anti rabbit IgG (H+L) (1:1000; #A27039; Invitrogen) and Alexa Fluor 488 goat anti chicken IgY (H+L) (1:1000; #A11039; Invitrogen). Nuclei were counterstained with 100 ng/ml Hoechst 33342 (Thermo Fisher). EdU incorporation was revealed using a Click-iT EdU Imaging Kit (Invitrogen Life Technologies) as per manufacturer's instructions. Myofibres were imaged on LSM Exciter confocal microscope (Zeiss) equipped with x40 objective. MPCs were imaged at x10 or x20 using an Axiovert 200M microscope (Zeiss). At least three random fields were acquired in each of three technical replicates. Differentiation index was calculated as: nuclei in $MyHC^{+}$ myocytes x 100/ total nuclei.

RNA extraction, RT-PCR and qPCR

Genotyped *myog*$^{kg125/+}$ (sib) or *myog*^{kg125} (*myog*$^{-/-}$) adult trunk muscles were triturated and processed for RNA extraction using RNA Purification Plus Kit (Norgen) following supplier's instructions. Total RNA was reverse transcribed using Superscript III reverse transcriptase (Invitrogen) following supplier's instructions. For MPCs, RNA extraction was performed at indicated time point using micro-RNA kit (Qiagen). Prior to collection, culture wells were washed 3 times with PBS to remove myofibres, followed by MPCs detachment using Accutase (Sigma Aldrich) for 10 minutes at 28.5 ºC. QPCR on technical triplicates for each sample was performed on 5 ng of relative RNA using Takyon Low ROX SYBR 2X MasterMix blue dTTP (Takyon) on a ViiA™7 thermal cycler (Applied Biosystems). Ct values of all genes analysed were normalized to the geometrical mean of Ct values of three housekeeping genes (*actinb2, sep15* and *b2m*) and fold changes were calculated using ΔΔCt method (Livak and Schmittgen, 2001). Results are presented as mean value ± SEM of fold changes from independent experiments as indicated. Used primers, purchased from Sigma-Aldrich (KiCqStart SYBR Green Primers Predesigned, Sigma Aldrich) are listed in Table S1.

Statistical analyses

Quantitative analysis on images was performed with Fiji (NIH, www.Fiji.sc) and ZEN (2009 + 2012) software. Statistical analyses were performed using GraphPad (Prism 6 or 8) or Microsoft Excel (v16) for unpaired or paired two-tailed Student's *t*-test as indicated and one-way ANOVA followed by Holm-Sidak's posthoc (growth mode analysis) or Bonferroni (MuSC analysis). χ^2 test was performed on raw data and used to assess difference between distributions.

Acknowledgements

We are grateful to all members of the Hughes lab and Zammit lab for advice and to Bruno Correia da Silva and his staff for care of the fish. This work is supported by grants from the Medical Research Council to S.M.H. (MRC Programme Grants G1001029 and MR/N021231/1) and P.S.Z. (MR/P023215/1 and MR/S002472/1), and from Muscular Dystrophy UK (RA3/3052), Association Française contre les Myopathies (AFM17865) and the FSH Society (FSHS-82013-06 and FSHS-82017-05) to P.S.Z.

Author contributions

MG and SMH conceived the project. MG designed and performed all experiments and analysis. MG established the protocol for culture of zebrafish adult MuSCs. SB performed qPCR assay and contributed to sample preparation for qPCR from adult tissue and cell culture. KW performed statistical analysis on muscle growth and contributed to fish genotyping. PSZ assisted in protocol establishment, experimental plan and provided cell culture reagents. MG and SMH wrote the paper with contributions from all other authors.

Declaration of Interests

The authors declare no competing interests.

References

Beauchamp, J.R., Heslop, L., Yu, D.S., Tajbakhsh, S., Kelly, R.G., Wernig, A., Buckingham, M.E., Partridge, T.A., and Zammit, P.S. (2000). Expression of CD34 and myf5 defines the majority of quiescent adult skeletal muscle satellite cells. J Cell Biol *151*, 1221-1234.

Berberoglu, M.A., Gallagher, T.L., Morrow, Z.T., Talbot, J.C., Hromowyk, K.J., Tenente, I.M., Langenau, D.M., and Amacher, S.L. (2017). Satellite-like cells contribute to pax7-dependent skeletal muscle repair in adult zebrafish. Dev Biol *424*, 162-180.

Blagden, C.S., Currie, P.D., Ingham, P.W., and Hughes, S.M. (1997). Notochord induction of zebrafish slow muscle mediated by Sonic Hedgehog. Genes Dev *11*, 2163-2175.

Brack, A.S., Bildsoe, H., and Hughes, S.M. (2005). Evidence that satellite cell decrement contributes to preferential decline in nuclear number from large fibres during murine age-related muscle atrophy. J Cell Sci *118*, 4813-4821.

Buckingham, M., and Relaix, F. (2015). PAX3 and PAX7 as upstream regulators of myogenesis. Semin Cell Dev Biol *44*, 115-125.

Cardasis, C.A., and Cooper, G.W. (1975). An analysis of nuclear numbers in individual muscle fibers during differentiation and growth: a satellite cell-muscle fiber growth unit. J Exp Zool *191*, 347-358.

Chakravarthy, M.V., Booth, F.W., and Spangenburg, E.E. (2001). The molecular responses of skeletal muscle satellite cells to continuous expression of IGF-1: implications for the rescue of induced muscular atrophy in aged rats. Int J Sport Nutr Exerc Metab *11 Suppl*, S44-48.

Chen, C., Liu, Y., Liu, R., Ikenoue, T., Guan, K.L., Liu, Y., and Zheng, P. (2008). TSC-mTOR maintains quiescence and function of hematopoietic stem cells by repressing mitochondrial biogenesis and reactive oxygen species. J Exp Med *205*, 2397-2408.

578 Chen, Y., Lin, G., and Slack, J.M. (2006). Control of muscle regeneration in the Xenopus tadpole tail by
579 Pax7. Development *133*, 2303-2313.

580 Coleman, M.E., DeMayo, F., Yin, K.C., Lee, H.M., Geske, R., Montgomery, C., and Schwartz, R.J. (1995).
581 Myogenic vector expression of insulin-like growth factor I stimulates muscle cell differentiation and
582 myofiber hypertrophy in transgenic mice. J Biol Chem *270*, 12109-12116.

583 Cooper, R.N., Tajbakhsh, S., Mouly, V., Cossu, G., Buckingham, M., and Butler-Browne, G.S. (1999). In vivo
584 satellite cell activation via Myf5 and MyoD in regenerating mouse skeletal muscle. J Cell Sci *112 (Pt*
585 *17)*, 2895-2901.

586 Cornelison, D.D., and Wold, B.J. (1997). Single-cell analysis of regulatory gene expression in quiescent and
587 activated mouse skeletal muscle satellite cells. Dev Biol *191*, 270-283.

588 Coutelle, O., Blagden, C.S., Hampson, R., Halai, C., Rigby, P.W., and Hughes, S.M. (2001). Hedgehog
589 signalling is required for maintenance of myf5 and myoD expression and timely terminal differentiation
590 in zebrafish adaxial myogenesis. Dev Biol *236*, 136-150.

591 Davis, G.K., D'Alessio, J.A., and Patel, N.H. (2005). Pax3/7 genes reveal conservation and divergence in the
592 arthropod segmentation hierarchy. Dev Biol *285*, 169-184.

593 Devoto, S.H., Stoiber, W., Hammond, C.L., Steinbacher, P., Haslett, J.R., Barresi, M.J., Patterson, S.E.,
594 Adiarte, E.G., and Hughes, S.M. (2006). Generality of vertebrate developmental patterns: evidence for
595 a dermomyotome in fish. Evol Dev *8*, 101-110.

596 DiBella, L.M., Park, A., and Sun, Z. (2009). Zebrafish Tsc1 reveals functional interactions between the cilium
597 and the TOR pathway. Human molecular genetics *18*, 595-606.

598 Durieux, A.C., Amirouche, A., Banzet, S., Koulmann, N., Bonnefoy, R., Pasdeloup, M., Mouret, C., Bigard,
599 X., Peinnequin, A., and Freyssenet, D. (2007). Ectopic expression of myostatin induces atrophy of
600 adult skeletal muscle by decreasing muscle gene expression. Endocrinology *148*, 3140-3147.

601 Ekmark, M., Gronevik, E., Schjerling, P., and Gundersen, K. (2003). Myogenin induces higher oxidative
602 capacity in pre-existing mouse muscle fibres after somatic DNA transfer. J Physiol *548*, 259-269.

603 Fiorotto, M.L., Schwartz, R.J., and Delaughter, M.C. (2003). Persistent IGF-I overexpression in skeletal
604 muscle transiently enhances DNA accretion and growth. FASEB J *17*, 59-60.

605 Flynn, J.M., Meadows, E., Fiorotto, M., and Klein, W.H. (2010). Myogenin regulates exercise capacity and
606 skeletal muscle metabolism in the adult mouse. PLoS One *5*, e13535.

607 Forcina, L., Miano, C., Pelosi, L., and Musaro, A. (2019). An Overview about the Biology of Skeletal Muscle
608 Satellite Cells. Curr Genomics *20*, 24-37.

609 Ganassi, M., Badodi, S., Ortuste Quiroga, H.P., Zammit, P.S., Hinits, Y., and Hughes, S.M. (2018).
610 Myogenin promotes myocyte fusion to balance fibre number and size. Nature communications *9*,
611 4232.

612 Ganassi, M., Badodi, S., Polacchini, A., Baruffaldi, F., Battini, R., Hughes, S.M., Hinits, Y., and Molinari, S.
613 (2014). Distinct functions of alternatively spliced isoforms encoded by zebrafish mef2ca and mef2cb.
614 Biochimica et biophysica acta *1839*, 559-570.

615 Gao, Y., Dai, Z., Shi, C., Zhai, G., Jin, X., He, J., Lou, Q., and Yin, Z. (2016). Depletion of Myostatin b
616 Promotes Somatic Growth and Lipid Metabolism in Zebrafish. Front Endocrinol (Lausanne) *7*, 88.

617 Gibson, M.C., and Schultz, E. (1982). The distribution of satellite cells and their relationship to specific fiber
618 types in soleus and extensor digitorum longus muscles. Anat Rec *202*, 329-337.

619 Hammond, C.L., Hinits, Y., Osborn, D.P., Minchin, J.E., Tettamanti, G., and Hughes, S.M. (2007). Signals
620 and myogenic regulatory factors restrict pax3 and pax7 expression to dermomyotome-like tissue in
621 zebrafish. Dev Biol *302*, 504-521.

622 Hasty, P., Bradley, A., Morris, J.H., Edmondson, D.G., Venuti, J.M., Olson, E.N., and Klein, W.H. (1993).
623 Muscle deficiency and neonatal death in mice with a targeted mutation in the myogenin gene. Nature
624 *364*, 501-506.

625 Hernandez-Hernandez, J.M., Garcia-Gonzalez, E.G., Brun, C.E., and Rudnicki, M.A. (2017). The myogenic
626 regulatory factors, determinants of muscle development, cell identity and regeneration. Semin Cell
627 Dev Biol *72*, 10-18.

628 Hinits, Y., Osborn, D.P., and Hughes, S.M. (2009). Differential requirements for myogenic regulatory factors
629 distinguish medial and lateral somitic, cranial and fin muscle fibre populations. Development *136*, 403-
630 414.

631 Hinits, Y., Williams, V.C., Sweetman, D., Donn, T.M., Ma, T.P., Moens, C.B., and Hughes, S.M. (2011).
632 Defective cranial skeletal development, larval lethality and haploinsufficiency in Myod mutant
633 zebrafish. Dev Biol *358*, 102-112.

634 Ho, D.K., I.; King, G.; Stuart, E. (2011). MatchIt: Nonparametric Preprocessing for Parametric Causal
635 Inference. J Stat Soft *42*, 1-28.

636 Hollway, G.E., Bryson-Richardson, R.J., Berger, S., Cole, N.J., Hall, T.E., and Currie, P.D. (2007). Whole-
637 somite rotation generates muscle progenitor cell compartments in the developing zebrafish embryo.
638 Dev Cell *12*, 207-219.

639 Hughes, S.M., and Blau, H.M. (1990). Migration of myoblasts across basal lamina during skeletal muscle
640 development. Nature *345*, 350-353.

641 Hughes, S.M., Chi, M.M., Lowry, O.H., and Gundersen, K. (1999). Myogenin induces a shift of enzyme
642 activity from glycolytic to oxidative metabolism in muscles of transgenic mice. J Cell Biol *145*, 633-642.

643 Hughes, S.M., Taylor, J.M., Tapscott, S.J., Gurley, C.M., Carter, W.J., and Peterson, C.A. (1993). Selective
644 accumulation of MyoD and myogenin mRNAs in fast and slow adult skeletal muscle is controlled by
645 innervation and hormones. Development *118*, 1137-1147.

646 Kawakami, A., Kimura-Kawakami, M., Nomura, T., and Fujisawa, H. (1997). Distributions of PAX6 and PAX7
647 proteins suggest their involvement in both early and late phases of chick brain development. Mech
648 Dev *66*, 119-130.

649 Keefe, A.C., Lawson, J.A., Flygare, S.D., Fox, Z.D., Colasanto, M.P., Mathew, S.J., Yandell, M., and Kardon,
650 G. (2015). Muscle stem cells contribute to myofibres in sedentary adult mice. Nature communications
651 *6*, 7087.

652 Kelu, J.J., Pipalia, T.G., and Hughes, S.M. (2019). Circadian regulation of muscle growth independent of
653 locomotor activity. bioRxiv, 778787.

654 Knapp, J.R., Davie, J.K., Myer, A., Meadows, E., Olson, E.N., and Klein, W.H. (2006). Loss of myogenin in
655 postnatal life leads to normal skeletal muscle but reduced body size. Development *133*, 601-610.

656 Kuang, S., Kuroda, K., Le Grand, F., and Rudnicki, M.A. (2007). Asymmetric self-renewal and commitment
657 of satellite stem cells in muscle. Cell *129*, 999-1010.

658 Latres, E., Amini, A.R., Amini, A.A., Griffiths, J., Martin, F.J., Wei, Y., Lin, H.C., Yancopoulos, G.D., and
659 Glass, D.J. (2005). Insulin-like growth factor-1 (IGF-1) inversely regulates atrophy-induced genes via
660 the phosphatidylinositol 3-kinase/Akt/mammalian target of rapamycin (PI3K/Akt/mTOR) pathway. J
661 Biol Chem *280*, 2737-2744.

662 Lindstrom, M., Pedrosa-Domellof, F., and Thornell, L.E. (2010). Satellite cell heterogeneity with respect to
663 expression of MyoD, myogenin, Dlk1 and c-Met in human skeletal muscle: application to a cohort of
664 power lifters and sedentary men. Histochem Cell Biol *134*, 371-385.

665 Livak, K.J., and Schmittgen, T.D. (2001). Analysis of relative gene expression data using real-time
666 quantitative PCR and the 2(-Delta Delta C(T)) Method. Methods *25*, 402-408.

667 Machado, L., Esteves de Lima, J., Fabre, O., Proux, C., Legendre, R., Szegedi, A., Varet, H., Ingerslev, L.R.,
668 Barres, R., Relaix, F.*, et al.* (2017). In Situ Fixation Redefines Quiescence and Early Activation of
669 Skeletal Muscle Stem Cells. Cell reports *21*, 1982-1993.

670 Mahalwar, P., Walderich, B., Singh, A.P., and Nüsslein-Volhard, C. (2014). Local reorganization of
671 xanthophores fine-tunes and colors the striped pattern of zebrafish. Science *345*, 1362-1364.

672 Manceau, M., Gros, J., Savage, K., Thome, V., McPherron, A., Paterson, B., and Marcelle, C. (2008).
673 Myostatin promotes the terminal differentiation of embryonic muscle progenitors. Genes Dev *22*, 668-
674 681.

675 Mashinchian, O., Pisconti, A., Le Moal, E., and Bentzinger, C.F. (2018). The Muscle Stem Cell Niche in
676 Health and Disease. Curr Top Dev Biol *126*, 23-65.

677 Mauro, A. (1961). Satellite cell of skeletal muscle fibers. J Biophys Biochem Cytol *9*, 493-495.

McCall, G.E., Allen, D.L., Linderman, J.K., Grindeland, R.E., Roy, R.R., Mukku, V.R., and Edgerton, V.R. (1998). Maintenance of myonuclear domain size in rat soleus after overload and growth hormone/IGF-I treatment. J Appl Physiol *84*, 1407-1412.

McCroskery, S., Thomas, M., Maxwell, L., Sharma, M., and Kambadur, R. (2003). Myostatin negatively regulates satellite cell activation and self-renewal. J Cell Biol *162*, 1135-1147.

McPherron, A.C., Lawler, A.M., and Lee, S.J. (1997). Regulation of skeletal muscle mass in mice by a new TGF-beta superfamily member. Nature *387*, 83-90.

Meadows, E., Cho, J.H., Flynn, J.M., and Klein, W.H. (2008). Myogenin regulates a distinct genetic program in adult muscle stem cells. Dev Biol *322*, 406-414.

Megeney, L.A., Kablar, B., Garrett, K., Anderson, J.E., and Rudnicki, M.A. (1996). MyoD is required for myogenic stem cell function in adult skeletal muscle. Genes Dev *10*, 1173-1183.

Moresi, V., Williams, A.H., Meadows, E., Flynn, J.M., Potthoff, M.J., McAnally, J., Shelton, J.M., Backs, J., Klein, W.H., Richardson, J.A.*, et al.* (2010). Myogenin and class II HDACs control neurogenic muscle atrophy by inducing E3 ubiquitin ligases. Cell *143*, 35-45.

Moretti, I., Ciciliot, S., Dyar, K.A., Abraham, R., Murgia, M., Agatea, L., Akimoto, T., Bicciato, S., Forcato, M., Pierre, P.*, et al.* (2016). MRF4 negatively regulates adult skeletal muscle growth by repressing MEF2 activity. Nature communications *7*, 12397.

Nabeshima, Y., Hanaoka, K., Hayasaka, M., Esumi, E., Li, S., Nonaka, I., and Nabeshima, Y. (1993). Myogenin gene disruption results in perinatal lethality because of severe muscle defect. Nature *364*, 532-535.

Nikolaou, S., Cramer, A.A., Hu, L., Goh, Q., Millay, D.P., and Cornwall, R. (2019). Proteasome inhibition preserves longitudinal growth of denervated muscle and prevents neonatal neuromuscular contractures. JCI Insight *4*.

Nobukini, T., and Thomas, G. (2004). The mTOR/S6K signalling pathway: the role of the TSC1/2 tumour suppressor complex and the proto-oncogene Rheb. Novartis Found Symp *262*, 148-154; discussion 154-149, 265-148.

Olguin, H.C., and Olwin, B.B. (2004). Pax-7 up-regulation inhibits myogenesis and cell cycle progression in satellite cells: a potential mechanism for self-renewal. Dev Biol *275*, 375-388.

Olguin, H.C., Yang, Z., Tapscott, S.J., and Olwin, B.B. (2007). Reciprocal inhibition between Pax7 and muscle regulatory factors modulates myogenic cell fate determination. J Cell Biol *177*, 769-779.

Oustanina, S., Hause, G., and Braun, T. (2004). Pax7 directs postnatal renewal and propagation of myogenic satellite cells but not their specification. EMBO J *23*, 3430-3439.

Pallafacchina, G., Blaauw, B., and Schiaffino, S. (2013). Role of satellite cells in muscle growth and maintenance of muscle mass. Nutr Metab Cardiovasc Dis *23 Suppl 1*, S12-18.

Patapoutian, A., Yoon, J.K., Miner, J.H., Wang, S., Stark, K., and Wold, B. (1995). Disruption of the mouse MRF4 gene identifies multiple waves of myogenesis in the myotome. Development *121*, 3347-3358.

Pinheiro, J.B., D.; DebRoy, S.; Sarkar, D.; R Core Team (2020). nlme: Linear and Nonlinear Mixed Effects Models. R package version 3, 1-147.

Pipalia, T.G., Koth, J., Roy, S.D., Hammond, C.L., Kawakami, K., and Hughes, S.M. (2016). Cellular dynamics of regeneration reveals role of two distinct Pax7 stem cell populations in larval zebrafish muscle repair. Dis Model Mech *9*, 671-684.

Porpiglia, E., Samusik, N., Ho, A.T.V., Cosgrove, B.D., Mai, T., Davis, K.L., Jager, A., Nolan, G.P., Bendall, S.C., Fantl, W.J.*, et al.* (2017). High-resolution myogenic lineage mapping by single-cell mass cytometry. Nat Cell Biol *19*, 558-567.

Powell-Braxton, L., Hollingshead, P., Warburton, C., Dowd, M., Pitts-Meek, S., Dalton, D., Gillett, N., and Stewart, T.A. (1993). IGF-I is required for normal embryonic growth in mice. Genes and Development *7*, 2609-2617.

Purohit, G., and Dhawan, J. (2019). Adult Muscle Stem Cells: Exploring the Links Between Systemic and Cellular Metabolism. Front Cell Dev Biol *7*, 312.

Quan, Z., Sun, P., Lin, G., and Xi, R. (2013). TSC1/2 regulates intestinal stem cell maintenance and lineage differentiation through Rheb-TORC1-S6K but independently of nutritional status or Notch regulation. J Cell Sci *126*, 3884-3892.

Rantanen, J., Hurme, T., Lukka, R., Heino, J., and Kalimo, H. (1995). Satellite cell proliferation and the expression of myogenin and desmin in regenerating skeletal muscle: evidence for two different populations of satellite cells. Lab Invest *72*, 341-347.

Rawls, A., Valdez, M.R., Zhang, W., Richardson, J., Klein, W.H., and Olson, E.N. (1998). Overlapping functions of the myogenic bHLH genes MRF4 and MyoD revealed in double mutant mice. Development *125*, 2349-2358.

Relaix, F., Montarras, D., Zaffran, S., Gayraud-Morel, B., Rocancourt, D., Tajbakhsh, S., Mansouri, A., Cumano, A., and Buckingham, M. (2006). Pax3 and Pax7 have distinct and overlapping functions in adult muscle progenitor cells. J Cell Biol *172*, 91-102.

Relaix, F., and Zammit, P.S. (2012). Satellite cells are essential for skeletal muscle regeneration: the cell on the edge returns centre stage. Development *139*, 2845-2856.

Riuzzi, F., Sorci, G., Sagheddu, R., Sidoni, A., Alaggio, R., Ninfo, V., and Donato, R. (2014). RAGE signaling deficiency in rhabdomyosarcoma cells causes upregulation of PAX7 and uncontrolled proliferation. J Cell Sci *127*, 1699-1711.

Rodgers, J.T., King, K.Y., Brett, J.O., Cromie, M.J., Charville, G.W., Maguire, K.K., Brunson, C., Mastey, N., Liu, L., Tsai, C.R.*, et al.* (2014). mTORC1 controls the adaptive transition of quiescent stem cells from G0 to G(Alert). Nature *510*, 393-396.

Roy, S.D., Williams, V.C., Pipalia, T.G., Li, K., Hammond, C.L., Knappe, S., Knight, R.D., and Hughes, S.M. (2017). Myotome adaptability confers developmental robustness to somitic myogenesis in response to fibre number alteration. Dev Biol *431*, 321-335.

Ruvinsky, I., Katz, M., Dreazen, A., Gielchinsky, Y., Saada, A., Freedman, N., Mishani, E., Zimmerman, G., Kasir, J., and Meyuhas, O. (2009). Mice deficient in ribosomal protein S6 phosphorylation suffer from muscle weakness that reflects a growth defect and energy deficit. PloS one *4*, e5618.

Schiaffino, S., and Mammucari, C. (2011). Regulation of skeletal muscle growth by the IGF1-Akt/PKB pathway: insights from genetic models. Skeletal muscle *1*, 4.

Schultz, E., Chamberlain, C., McCormick, K.M., and Mozdziak, P.E. (2006). Satellite cells express distinct patterns of myogenic proteins in immature skeletal muscle. Dev Dyn *235*, 3230-3239.

Seale, P., Sabourin, L.A., Girgis-Gabardo, A., Mansouri, A., Gruss, P., and Rudnicki, M.A. (2000). Pax7 is required for the specification of myogenic satellite cells. Cell *102*, 777-786.

Seger, C., Hargrave, M., Wang, X., Chai, R.J., Elworthy, S., and Ingham, P.W. (2011). Analysis of Pax7 expressing myogenic cells in zebrafish muscle development, injury, and models of disease. Dev Dyn *240*, 2440-2451.

Sekhon, J.S. (2011). Multivariate and Propensity Score Matching Software with Automated Balance Optimization: The Matching Package for R. J Stat Soft *42*, 1-52.

Shi, J., Cai, M., Si, Y., Zhang, J., and Du, S. (2018). Knockout of myomaker results in defective myoblast fusion, reduced muscle growth and increased adipocyte infiltration in zebrafish skeletal muscle. Human molecular genetics *27*, 3542-3554.

Soleimani, V.D., Punch, V.G., Kawabe, Y., Jones, A.E., Palidwor, G.A., Porter, C.J., Cross, J.W., Carvajal, J.J., Kockx, C.E., van, I.W.F.*, et al.* (2012). Transcriptional dominance of Pax7 in adult myogenesis is due to high-affinity recognition of homeodomain motifs. Dev Cell *22*, 1208-1220.

Trendelenburg, A.U., Meyer, A., Rohner, D., Boyle, J., Hatakeyama, S., and Glass, D.J. (2009). Myostatin reduces Akt/TORC1/p70S6K signaling, inhibiting myoblast differentiation and myotube size. Am J Physiol Cell Physiol *296*, C1258-1270.

Venuti, J.M., Morris, J.H., Vivian, J.L., Olson, E.N., and Klein, W.H. (1995). Myogenin is required for late but not early aspects of myogenesis during mouse development. J Cell Biol *128*, 563-576.

Voytik, S.L., Przyborski, M., Badylak, S.F., and Konieczny, S.F. (1993). Differential expression of muscle regulatory factor genes in normal and denervated adult rat hindlimb muscles. Dev Dyn *198*, 214-224.

Weintraub, H., Dwarki, V.J., Verma, I., Davis, R., Hollenberg, S., Snider, L., Lassar, A., and Tapscott, S.J. (1991). Muscle-specific transcriptional activation by MyoD. Genes Dev *5*, 1377-1386.

779 Westerfield, M. (2000). The Zebrafish Book - A guide for the laboratory use of zebrafish (Danio rerio)
780 (University of Oregon Press).

781 Yoon, M.S. (2017). mTOR as a Key Regulator in Maintaining Skeletal Muscle Mass. Front Physiol *8*, 788.

782 Zammit, P.S. (2017). Function of the myogenic regulatory factors Myf5, MyoD, Myogenin and MRF4 in
783 skeletal muscle, satellite cells and regenerative myogenesis. Semin Cell Dev Biol *72*, 19-32.

784 Zammit, P.S., Golding, J.P., Nagata, Y., Hudon, V., Partridge, T.A., and Beauchamp, J.R. (2004). Muscle
785 satellite cells adopt divergent fates: a mechanism for self-renewal? J Cell Biol *166*, 347-357.

786 Zammit, P.S., Heslop, L., Hudon, V., Rosenblatt, J.D., Tajbakhsh, S., Buckingham, M.E., Beauchamp, J.R.,
787 and Partridge, T.A. (2002). Kinetics of myoblast proliferation show that resident satellite cells are
788 competent to fully regenerate skeletal muscle fibers. Exp Cell Res *281*, 39-49.

789 Zammit, P.S., Relaix, F., Nagata, Y., Ruiz, A.P., Collins, C.A., Partridge, T.A., and Beauchamp, J.R. (2006).
790 Pax7 and myogenic progression in skeletal muscle satellite cells. J Cell Sci *119*, 1824-1832.

791 Zeileis, A.H., T. (2002). Diagnostic Checking in Regression Relationships. R News *2*, 7-10.

792 Zhang, L., Wang, X.H., Wang, H., Du, J., and Mitch, W.E. (2010). Satellite cell dysfunction and impaired IGF-
793 1 signaling cause CKD-induced muscle atrophy. J Am Soc Nephrol *21*, 419-427.

794 Zhang, W., Behringer, R.R., and Olson, E.N. (1995). Inactivation of the myogenic bHLH gene MRF4 results
795 in up-regulation of myogenin and rib anomalies. Genes Dev *9*, 1388-1399.

796 Zimmers, T.A., Davies, M.V., Koniaris, L.G., Haynes, P., Esquela, A.F., Tomkinson, K.N., McPherron, A.C.,
797 Wolfman, N.M., and Lee, S.J. (2002). Induction of cachexia in mice by systemically administered
798 myostatin. Science *296*, 1486-1488.

799

800

Figure Legends

Figure 1. Myogenin is required for normal myofibre size and nuclear accretion.

A. Schematic of trunk muscle processing for analysis, colours identify sib (*myog*$^{kg125/+}$, blue) or *myog*$^{-/-}$ (*myog*^{kg125}, red) samples throughout the figure.

B. qPCR analysis shows downregulation of *myog*, *mymk*, *mymx* and *mrf4* expression in adult *myog*$^{-/-}$. Symbol shapes denote paired sib and *myog*$^{-/-}$ samples, n=4-6 fish/genotype, paired *t*-test.

C. Schematic of myofibre isolation for morphometric analysis (top) and representative images (bottom) showing smaller *myog*$^{-/-}$ myofibre (red brackets) compared to age-matched sib. Scale bar=100 μm.

D. Measure of absolute myofibre length, n=3 fish/genotype, n=110-120 myofibres/fish, unpaired *t*-test.

E. Representative images and measure of unaltered sarcomere length on freshly-isolated myofibres, n=3 fish/genotype, n=10 myofibres/fish, unpaired *t*-test. Scale bar=10 μm.

F. Representative images of isolated fixed adult myofibres show size reduction in *myog*$^{-/-}$ (red bracket). Scale bar=100 μm.

G-J. Quantification of number of nuclei/100 μm (G), absolute number of nuclei per myofibre (H), myofibre diameter (I), and SADS (Surface Area Domain Size) (J) showing significant changes in myofibres from juvenile (Juv, 1 month-old) and adult (Ad, 8 months-old) stages within (coloured *p*) or among (black *p*) genotypes. n=3 fish/genotype, n=30-50 adult myofibres/fish, n=15-20 juvenile myofibres/fish, one-way ANOVA.

K. Relationship of number of nuclei and $\log_e$(Surface Area) indicates different growth mode between sib and *myog*$^{-/-}$ (i.e. significant slope difference, black *p*), despite significant correlation $\log_e$(SA)/nuclei within genotype (coloured *p*) (see Methods).

L. Increase in surface area (SA) from juvenile to adult stage (= Ad_SA – Juv_SA) indicates reduced growth rate in *myog*$^{-/-}$. Data from Figure S1E, unpaired *t*-test.

All graphs report mean ± SEM. Statistical significance within (coloured *p*) or between (black *p*) genotypes is indicated.

Figure 2. Lack of Myogenin alters MuSC number and localisation.

Colours identify sib (blue) or *myog*$^{-/-}$ (red) samples throughout the figure.

A. qPCR analysis showing upregulation of *pax7a*, *pax7b*, *myf5* and unaltered *myod* in adult *myog*$^{-/-}$ mutant. Symbol shapes denote paired sib and *myog*$^{-/-}$ samples, n=6 fish/genotype, paired *t*-test.

B. Schematic of myofibre isolation for GFP^{+ve} cells analysis from *pax7a:GFP*;*myog*$^{-/-}$ and sib muscles.

C. Representative images showing GFP^{+ve} cells on sib (blue arrowhead) or *myog*$^{-/-}$ (red arrowheads) on isolated myofibres. Scale bar=100 μm.

D. Representative immunodetection of GFP (green), DP312 (magenta) and nuclei (white) on freshly-isolated adult sib or *myog*$^{-/-}$ myofibres. Scale bar=5 μm.

E,**F**. Quantification of absolute number of GFP^{+ve} cells (bona fide MuSC) per myofibre and myonuclear domain size. n=3 fish/genotype, n=20-30 myofibres/fish, unpaired *t*-test.

G. Pie charts showing the fraction of nuclei (left) and fraction of myofibres (right) with the indicated number of nuclei in GFP^{+ve} cells/myofibre in sib (blue stroke) and *myog*$^{-/-}$ (red stroke). Data from Figure S2G.

H. Diagram of measure of GFP^{+ve} cell distance from nearest myofibre-end (top). Each myofibre was segmented in tenths, where 1/10 and 5/10 corresponded to the segments nearest to and furthest from the

myofibre-end, respectively. Quantification of fraction of MuSC located within each myofibre segment (bottom, see Methods and Figure S2H). n=3 fish/genotype, n=30-50 MuSCs, *p*-value indicates probability of rejecting null hypothesis of no difference between *myog*$^{-/-}$ and sib in χ^2 test.

I. Representative images showing localization of the GFP^{+ve} cell on sib (blue rectangle) or *myog*$^{-/-}$ (red rectangle) mono-MuSC myofibres (with only one GFP^{+ve} cell). Scale bar=100 μm (=20 μm in 2x-zoom).

J. Quantification of fraction of MuSC located within each 10 μm segment from mono-MuSC myofibre-end. n=3 fish/genotype, n=15-25 MuSCs, black *p*-value indicates probability of rejecting null hypothesis of no difference between *myog*$^{-/-}$ and sib in χ^2 test. Coloured p-values indicate one-way ANOVA analysis of non-random MuSC distribution in 10 μm segments within each genotype. Magenta inset reports fraction of sib and *myog*$^{-/-}$ MuSC within the 0-9 and 10-19μm segments, unpaired *t*-test.

All graphs report mean ± SEM.

Figure 3. *Myog*$^{-/-}$ mutant muscle and MuSCs display enhanced mTORC1 signalling.

A. Schematic of adult trunk muscle processing for analysis. Colours identify sib (blue) or *myog*$^{-/-}$ (red) samples throughout.

B. qPCR analysis shows upregulation of *igf1* and downregulation of *mstnb* in *myog*$^{-/-}$ muscle. Symbol shapes denote paired sib and *myog*$^{-/-}$ samples, n=4 fish/genotype, paired *t*-test.

C. Summary of mTORC1 pathway with analysed members, positive (arrows) or negative (bars) effects are indicated. Dashed lines indicate other molecules involved; red dots represent phosphorylation events.

D. Western blot (left) and quantification (right) of phosphorylated/pan AKT (pAKT, Ser473) ratio and phosphorylated/pan RPS6 (pRPS6, Ser240/244). pRPS6 is increased in *myog*$^{-/-}$ muscle, n=3 fish/genotype, unpaired *t*-test. Actin immunoreactivity was used to normalise pan and phospho signals to protein loading prior to calculation of sample-specific phospho/pan ratio.

E. Representative images of myofibre immunostained for GFP (green), pRPS6 (red) and nuclei (white) fixed freshy immediately after isolation. Arrowheads indicate MuSCs on sib (blue) or *myog*$^{-/-}$ (red) myofibres. Dashed magenta squares highlight 4x-magnified cells. Scale bar=100 μm (=5 μm in 4x-zoom).

F. Quantification of pRPS6 intensity shows increase in *myog*$^{-/-}$ MuSCs. Symbol shapes denote paired sib and *myog*$^{-/-}$ samples, n=4 fish/genotype, n=20-30 MuSCs/fish, paired *t*-test.

G. qPCR analysis showing downregulation of *tsc1a* and *tsc1b* mRNAs while unaltered *tsc2* in *myog*$^{-/-}$ muscle. Symbol shapes denote paired sib and *myog*$^{-/-}$ samples, n=4-6 fish/genotype, paired *t*-test.

All graphs report mean ± SEM.

Figure 4. *Myog*$^{-/-}$ mutant MPCs exhibit faster entrance into proliferation phase.

A. Schematic of adult single myofibre culture and representative immunodetection of GFP (green) and nuclei (white) on cultured MPCs. Colours identify sib (blue) or *myog*$^{-/-}$ (red) samples throughout the figure.

B. Quantification of GFP^{+ve} cells obtained by single myofibre culture revealed increased MPCs yield from *myog*$^{-/-}$ after 4 days in growth medium, n=3 fish/genotype, n=8 myofibres/fish. Unpaired *t*-test on average MPCs/fish/genotype.

C. Percentage of GFP^{+ve} cells on total number of cells obtained, n=3 fish/genotype, unpaired *t*-test.

D. Relative proliferation rates of sib or *myog*$^{-/-}$ MPCs calculated as the ratio of the average number of GFP^{+ve} MPCs/plated-myofibre obtained in culture on the average number of GFP^{+ve} MuSCs/myofibre, unpaired *t*-test.

E. Diagram of myofibres culture and EdU pulse regime (top). Quantification of percentage of EdU^{+ve} MPCs at indicated time points (bottom left), symbol shapes denote MPCs obtained from same sib and *myog*$^{-/-}$ samples, n=3. Measurement of Area Under Curve (AUC, coloured area underneath dashed blue or red lines) to compare overall proliferation dynamics indicates reduction in *myog*$^{-/-}$ MPCs (bottom right), unpaired *t*-test.

F. Representative images of sib and *myog*$^{-/-}$ MPCs EdU incorporation at indicated time in culture, showing detection of EdU (red) and nuclei (blue).

G. qPCR analysis shows expression dynamics of *pax7a*, *pax7b*, *myod* and *myf5* mRNAs in sib and *myog*$^{-/-}$ MPCs cultured for 2 (n=4) or 3 days (n=3), unpaired *t*-test.

H. qPCR analysis indicating upregulation of *mef2d* and *mylpfa* mRNAs in *myog*$^{-/-}$ MPCs at 3 days of culture in growth medium. n=3, unpaired *t*-test.

I. Representative immunodetection of MyHC (red) and nuclei (white) on sib or *myog*$^{-/-}$ MPCs at 3 days (left). Extent of differentiation ((%) Index, see Methods) is higher in *myog*$^{-/-}$ MPCs cultured as in H (right).

All graphs report mean ± SEM. Statistical significance within (coloured *p*) or between (black *p*) genotypes is indicated. Scale bars=100 μm

Figure S1. *Myog*^{kg125} mutant adult and juvenile myofibres are smaller.

A. Fraction of adult myofibres (%) with indicated length in sib (blue, *myog*$^{kg125/+}$) and *myog*$^{-/-}$ (red, *myog*^{kg125}). n=3 fish/genotype, n=110-120 myofibres/fish, *p*-value indicates probability of rejecting null hypothesis of no difference between *myog*$^{-/-}$ and sib in χ^2 test.

B. Measure of absolute 1 month-old juvenile myofibre length, n=3 fish/genotype, unpaired *t*-test (left) and fraction of juvenile myofibres (%) with indicated length in sib (blue) and *myog*$^{-/-}$ (red), n=3 fish/genotype, n=15-20 juvenile myofibres/fish, *p*-value indicates probability of rejecting null hypothesis of no difference between *myog*$^{-/-}$ and sib in χ^2 test. (right).

C. Measure of absolute adult myofibre length, n=3 fish/genotype, n=100 myofibres/fish, unpaired *t*-test; sib (blue, *myog*$^{fh265/+}$), hypomorphic mutant (cyan, *myog*^{fh265}).

D. Representative images showing sib and *myog*$^{-/-}$ juvenile myofibres (left), scale bar=100 µm. Quantification of absolute number of nuclei per juvenile myofibre. n=3 fish/genotype, n=15-20 myofibres/fish, unpaired *t*-test.

E. Quantification of average myofibre diameter showing significant changes at juvenile (Juv) and adult (Ad) stages within (coloured *p*) or among (black *p*) genotypes. n=3 fish/genotype, n=30-50 adult myofibre/fish, n=15-20 juvenile myofibre/fish, one-way ANOVA.

Figure S2. *pax7a:GFP;myog*^{kg125} muscle is smaller and displays altered MuSC cellularity and unchanged *Pax3* genes expression.

A. Schematic of trunk muscle processing for qPCR analysis (left), sib (blue), *myog*$^{-/-}$ (red). Expression of *pax3a* and *pax3b* mRNA is unchanged in *myog*$^{-/-}$ muscle (right). Symbol shapes denote paired sib and *myog*$^{-/-}$ samples, n=6 fish/genotype, paired *t*-test.

B. Representative images of adult *pax7a:GFP;myog*$^{+/-}$ (sib) and *pax7a:GFP; myog*$^{-/-}$ (left) and show reduced length, weight, body mass index and standard weight in *myog*$^{-/-}$ compared to co-reared sibs (right), n=7, unpaired *t*-test. Scale bar=1 cm.

C. Schematic of *pax7a:GFP* adult trunk muscle processing for MuSC analysis (left). Fraction of GFP^{+ve} cells (bona fide MuSC) per myofibre is significantly increased in *myog*$^{-/-}$ muscle (right). n=3 fish/genotype, unpaired *t*-test.

D. Quantification of absolute number of (non-MuSC) myonuclei per adult myofibre. n=3 fish/genotype, n=20-30 myofibres/fish, unpaired *t*-test.

E,F. Quantification of absolute myofibre volume and myonuclear SADS (Surface Area Domain Size). n=3 fish/genotype, n=20-30 myofibres/fish, unpaired *t*-test.

G. Fraction of myofibres (%) with indicated number of GFP^{+ve} cells, n=3 fish/genotype, n=20-30 myofibres/fish, *p*-value indicates probability of rejecting null hypothesis of no difference between *myog*$^{-/-}$ and sib in χ^2 test.

H. Schematic of GFP^{+ve} cell distance to nearest myofibre-end measurement (left). Note that while average half-length (in magenta) of sib myofibre (blue diagram) is 500 µm, *myog*$^{-/-}$ myofibre average half-length is 250 µm (red diagram). To compare absolute distance to myofibre-end, each myofibre was segmented into 50 µm segments and the fraction of GFP^{+ve} cells (%) within each distance segment from nearest myofibre-end plotted, n=3 fish/genotype, n=20-30 MuSCs/fish, *p*-value indicates probability of rejecting null hypothesis of no difference between *myog*$^{-/-}$ and sib in χ^2 test.

All graphs report mean ± SEM.

940 **Figure S3. Characteristics of cultured MPCs and expression levels of *igfr1a* and *igfr1b.***

941 **A**. Schematic of adult trunk muscle processing for qPCR analysis (left). Summary of mTORC1 pathway with
942 analysed members, positive (arrows) or negative (bars) effects are indicated. Dashed lines indicate other
943 molecules involved, plain arrow indicate direct effect, red dots represent phosphorylation (middle). *Igfr1a* and
944 *igfr1b* are unchanged in *myog*$^{-/-}$ muscle compared to sib (right). Symbol shapes denote paired sib and *myog*$^{-/-}$
945 samples, n=5 fish/genotype, paired *t*-test.
946 **B**. Schematic of single-myofibre culture and analysis of derived MPCs (left) after 4 days from plating in growth
947 medium. Total number of cells (= GFP^{+ve} + GFP^{-ve}) is increased in *myog*$^{-/-}$ (middle). n=3 fish/genotype, n=8
948 myofibre/fish. Unpaired *t*-test on average cells/fish/genotype. Representative immunostaining of Desmin (red)
949 and nuclei (white) confirming myogenic identity of both sib and *myog*$^{-/-}$ cells (right) from single-plated myofibres.
950 **C**. Schematic of 90-100 myofibres culture and analysis of derived MPCs (left). Representative immunostaining
951 of Desmin (red), GFP (green) and nuclei (white) confirming myogenic identity of both sib and *myog*$^{-/-}$ cells after
952 2 days of culture (middle). *Myog*$^{-/-}$ myofibres yielded higher number of Desmin^{+} MPCs per field of view (FOV).
953 Symbol shapes denote paired sib and *myog*$^{-/-}$ samples, n=3 fish/genotype, paired *t*-test (right).
954 **D**. 90-100 myofibres culture from both genotypes yielded over 90% of Desmin^{+} cells, confirming high purity of
955 the myogenic population, n=3 fish/genotype, unpaired *t*-test.
956 All graphs report mean ± SEM. Scale bars=100 μm.

qPCR primers

gene	Forward 5'-3'	Reverse 5'-3'
actinb2	ATCCTTCTTGGGTATGGAAT	GACAATACAGTGTTGGCATA
sep15	CTCAAGTCCAAGCTTTTGTC	AGCCTCTCACATACTTGATT
b2m	TTGGCTCTCTCGAATAAAAC	CTTTCGGAGTGGAGACTTTC
myod	AACATTACAGTGGAGACTCTG	GTCATAGCTGTTCCGTCTTC
myf5	ATGGCCTCAGATGAATCAAA	CATTGTGCTAGCATTTTGTG
mrf4	CAGGAGAACCCAGATCATTC	GGACTCTGAAGACTCCAAC
myog	TCAGAAACACCCACAAACGCTCAC	GCAGGCCCAGGGGAGACACT
pax7a	CAAGAAAGATGACGATGACG	GTGCGATTACCTTTATCCC
pax7b	CGGGATACCAGTATAGTCAG	CATTCTTTGCCAGGTAATCC
pax3a	TTCCTTCAGTGAGTTCCATC	CGTTTCCACCAAATTTACAG
pax3b	CACTCACAATAACAACGCTA	ATGGAGTTATCAGTCCCATC
myomaker	GGACAACTTATTCACAGGGA	TCTGTGATTTTGACAAGCAG
myomixer	TCTGGTTGTCCGACTCTTCG	TTAAGAAGGCACAGGACGCA
mef2d	TCAAACAAGCTCTTCCAGTA	GTGCTCTTTCTTGTTCAGAG
mylpfa	TCCCTTTCTTGCTTTCTACC	GAAAACAATCCAATGTCCCC
igf1	GGCTTTTATTTCAGCAAACC	GTTGTGTGACCTTCTTGAAC
igfr1a	GATGTCTCCAGAGTCTTTGA	CATAAAACCACACCAAACGA
igfr1b	GTGTACATTCGCACTAAACC	TGAAGAATTAGCGTATGCAC
myostatinb	CAAGACACTGTGCAATAGAA	CATAGTCATATGAAGCGGTG
tsc1a	CATTAATGGCAGTCAGGAAG	GAAATGAATGAGTAAGGGCG
tsc1b	AAGAACATTTTCCACTCGAC	AAGACACAAGGTCCAATCAT
tsc2	AAACTAGAGTCTCAGTCCAG	GCATGACCACCTGATATAGA

Figure 1 Ganassi et al.

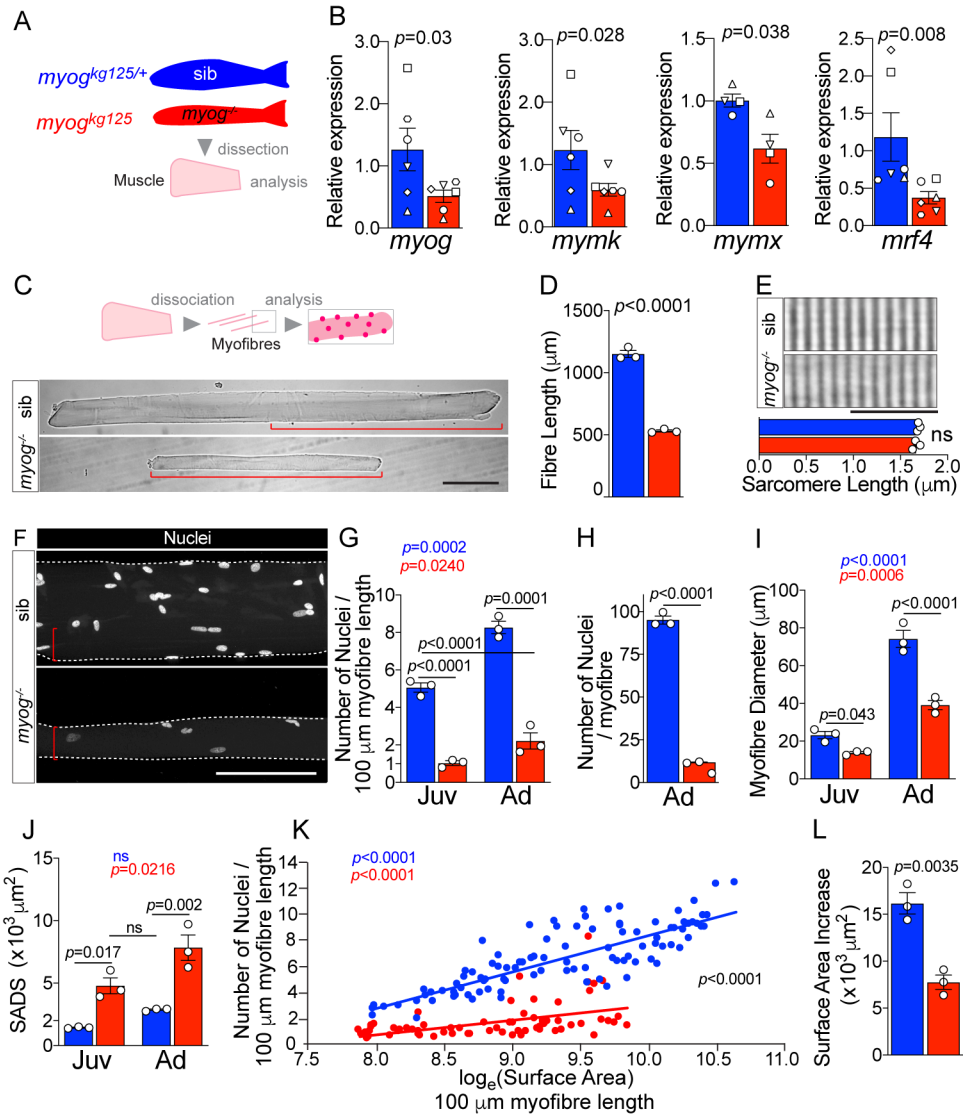

Figure 2

Ganassi et al.

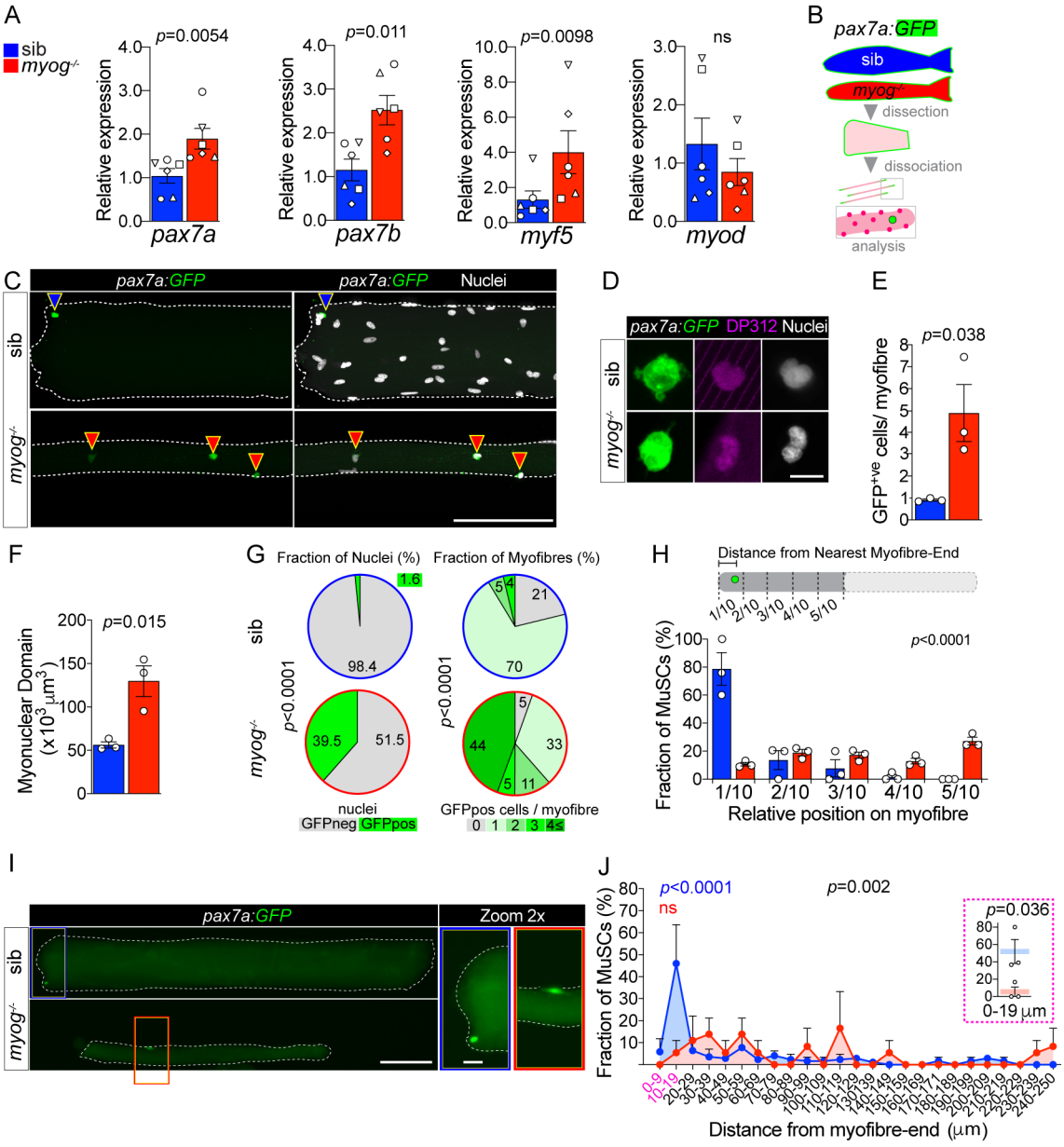

Figure 3 Ganassi et al.

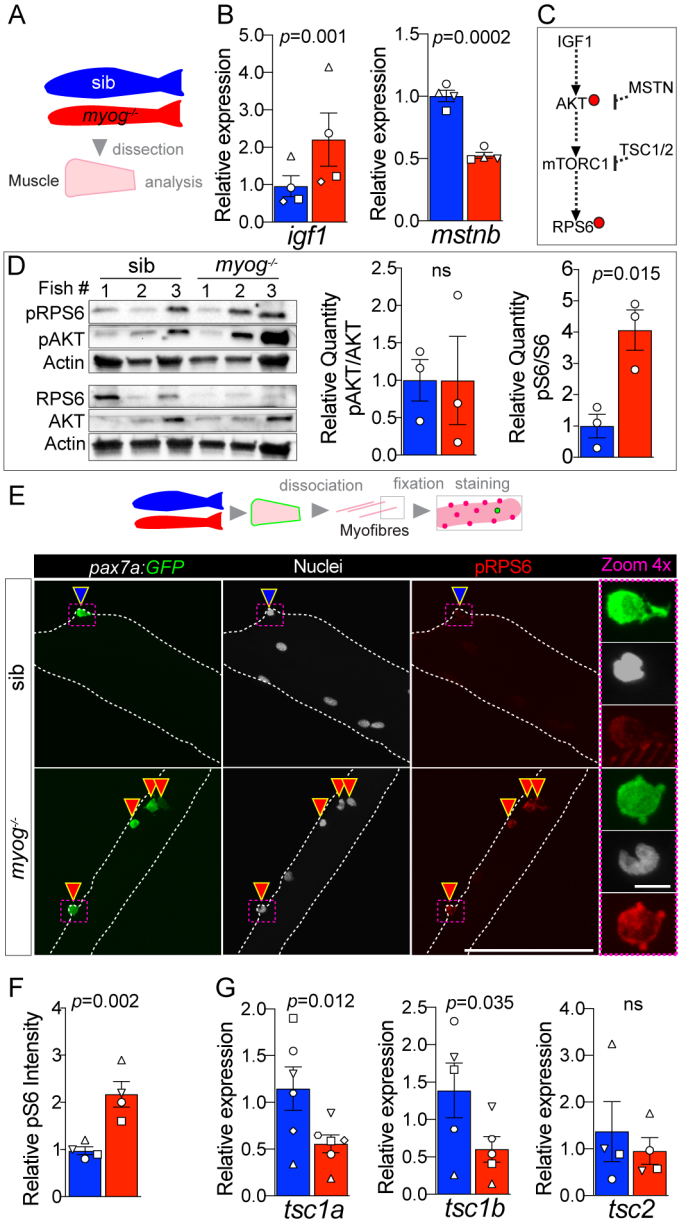

Figure 4 Ganassi et al.

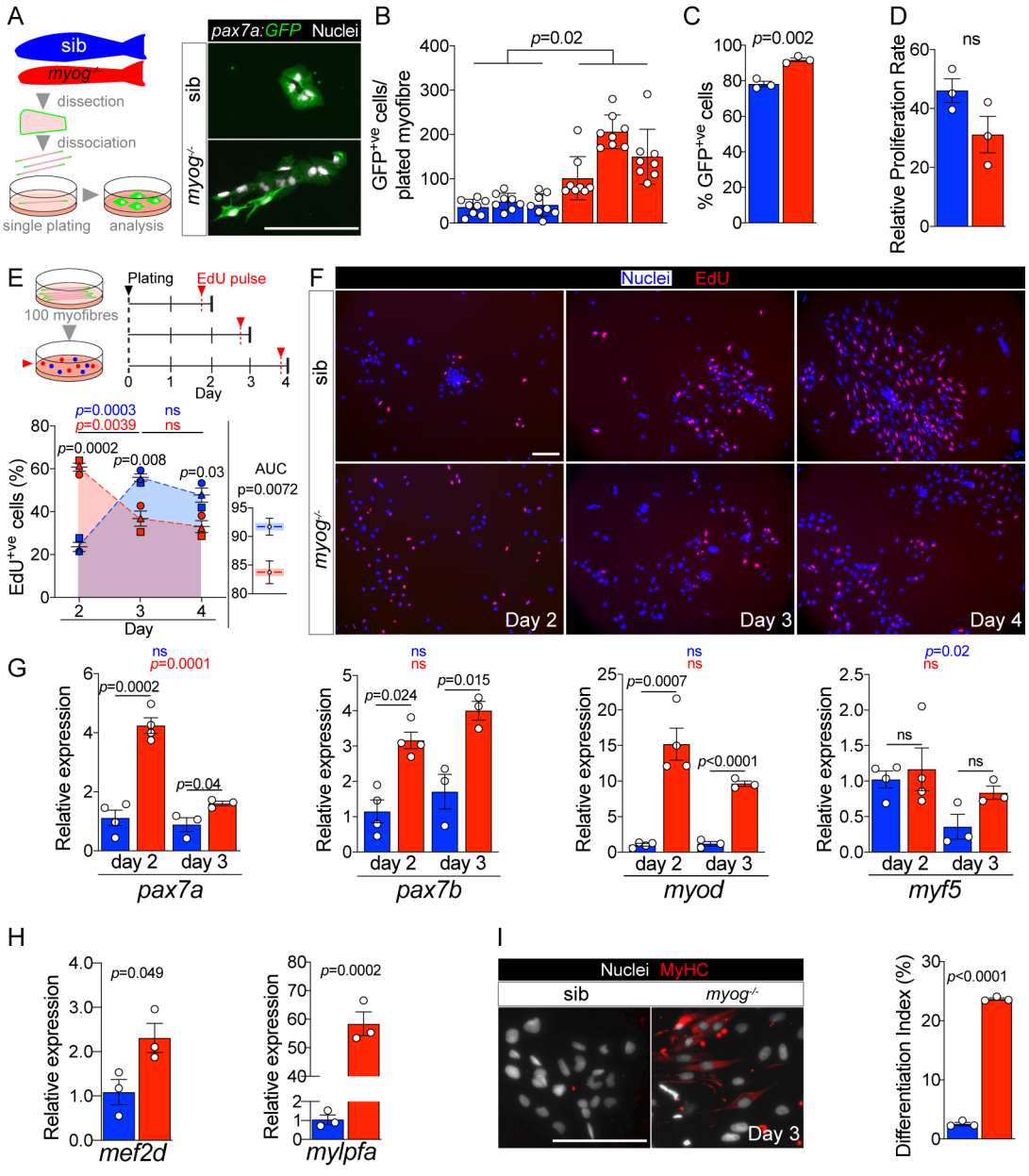

Figure S1

Ganassi et al.

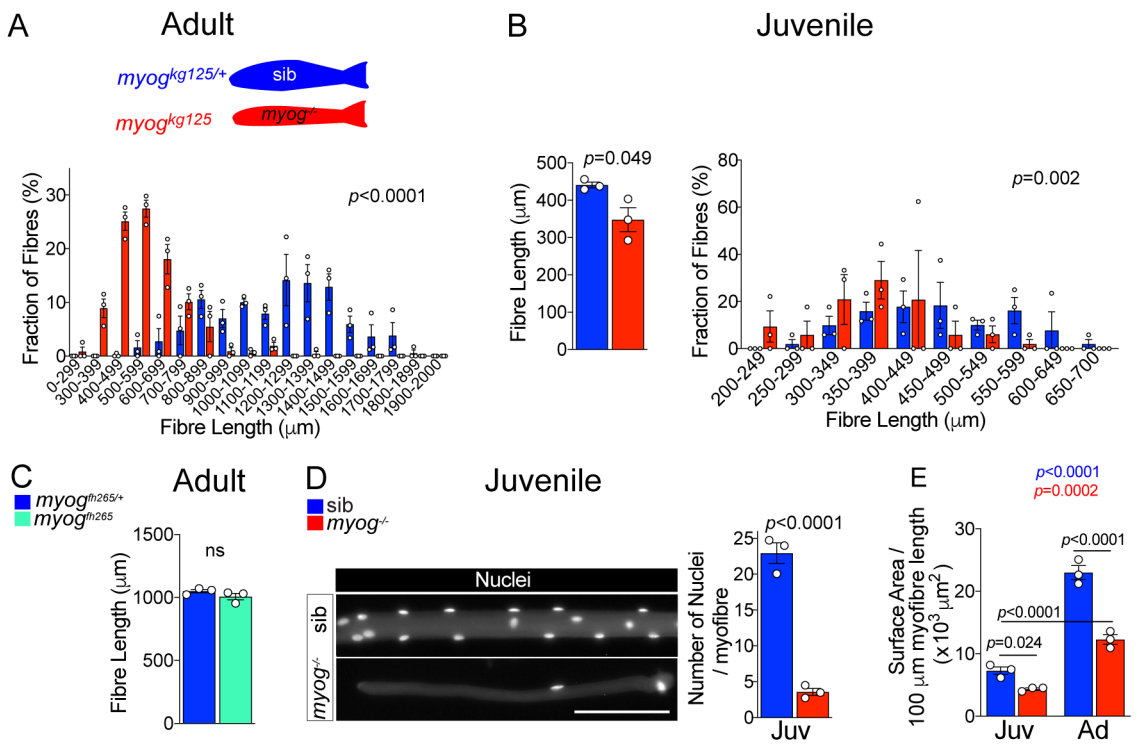

Figure S2

Ganassi et al.

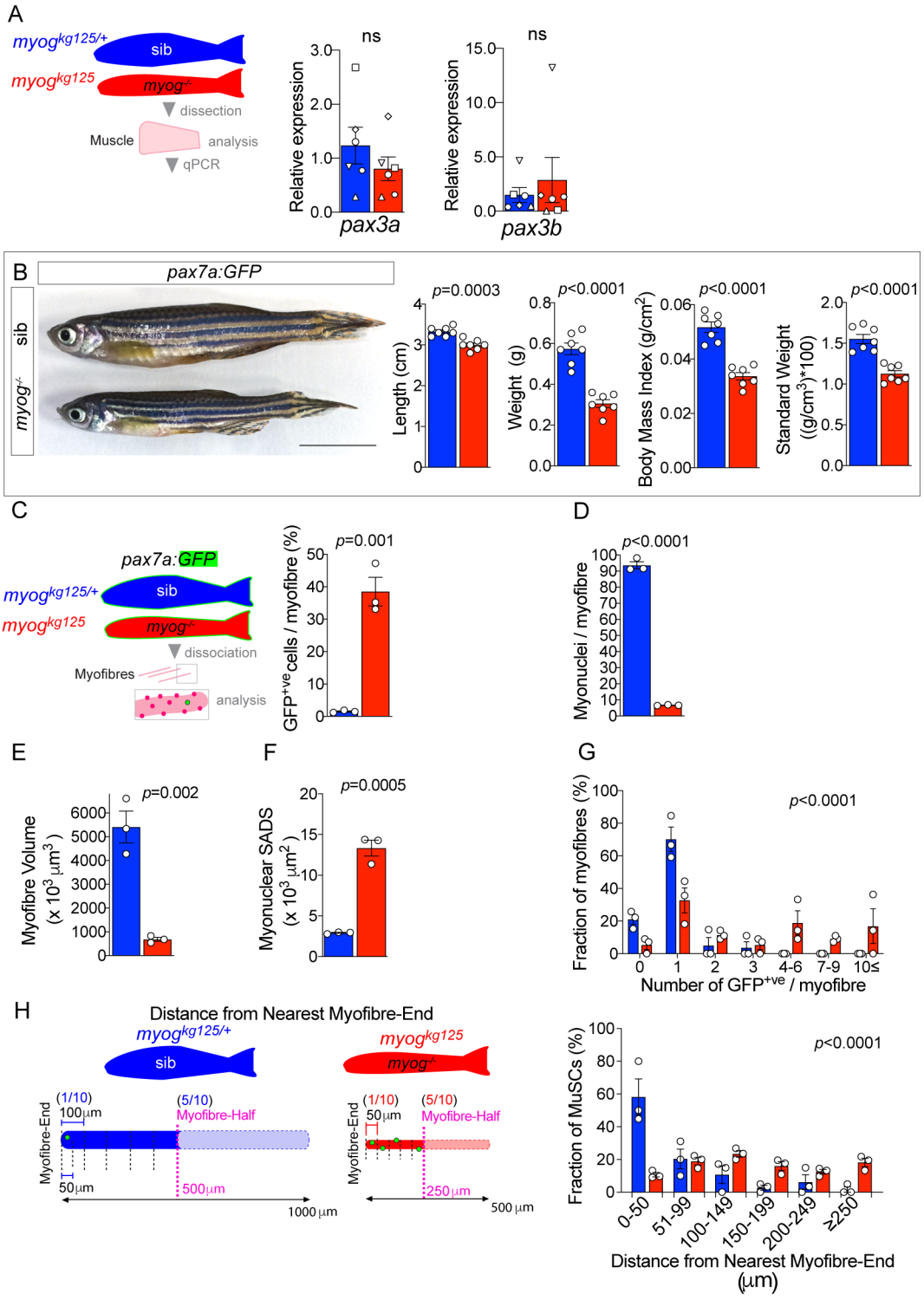

Figure S3

Ganassi et al.